NRL Report 8327

The NRL-EPRI Research Program (RP886-2), Evaluation and Prediction of Neutron Embrittlement in Reactor Pressure Vessel Materials, Annual Progress Report for CY 1978

J. R. HAWTHORNE, EDITOR

Thermostructural Materials Branch
Material Science and Technology Division

August 30, 1979

NAVAL RESEARCH LABORATORY
Washington, D.C.

20. Abstract (Continued)

for the benefit of reactor vessel design and operation. A primary objective of this program is the development of a high-quality data base for the evaluation of current radiation-embrittlement projection methods and the development of improved methods.

This report documents program highlights and research results for CY 1978 along with plans for the third-year investigation. Principal results include completion of half of the scheduled program irradiation experiments as well as commencement of postirradiation notch ductility and fracture toughness testing. The facility and procedures developed for *J-R* curve testing of irradiated compact toughness specimens are described. Postirradiation results are presented for four experiments which contained A533-B steel plate material.

CONTENTS

THE NRL-EPRI RESEARCH PROGRAM (RP886-2), EVALUATION AND PREDICTION OF NEUTRON EMBRITTLEMENT IN REACTOR PRESSURE VESSEL MATERIALS, ANNUAL PROGRESS REPORT FOR CY 1978

SUMMARY

The NRL-EPRI RP886-2 Research Program was formalized in January 1977. This report documents the highlights and accomplishments of the NRL investigations during CY 1978, the second year of program operation.

The program was designed as a 3-year effort and focuses on radiation-induced changes to reactor pressure vessel materials typical of past as well as current commercial production. Radiation effects are being investigated by standard Charpy-V (C_v), fatigue precracked Charpy-V (PCC_v), and compact toughness (CT) test methods. Primary accomplishments during CY 1978 relate to material acquisitions and specimen fabrication, expansion of the irradiation facility, conduct of material irradiation experiments, and performance of initial postirradiation material evaluations.

Highlights of material evaluations during this reporting period include:

- Observation of a general agreement between C_v 41-J and K_{Jd} 99-MPa$\sqrt{m}$ transition-temperature elevations measured by postirradiation C_v, PCC_v, and CT test methods. The suggested correlation, if confirmed by additional irradiation data, will be of major value to the interpretation and use of C_v results from reactor vessel surveillance.

- Observation of good agreement between postirradiation C_v 41-J transition-temperature elevations measured for A533-B steel and projections of transition-temperature changes by irradiation computed from NRC Regulatory Guide 1.99. The data indicate that the Guide is not highly conservative for the materials and fluence conditions evaluated.

- First indication of a significant difference in radiation embrittlement sensitivity between A533-B steel produced in the United States and that produced overseas. The tentative finding suggests a detrimental effect of high arsenic content on steel radiation resistance.

- Formulation of an alternative experimental definition of J_{Ic} for reactor vessel materials. Observations indicate that the proposed ASTM standard method for J_{Ic} definition lacks sufficient precision to resolve J_{Ic} for cases of limited crack extension and cleavage instability. The alternative method overcomes this inadequacy.

Manuscript submitted May 11, 1979.

- Development of a new definition of upper shelf initiation toughness. The proposed definition is based on a small (0.15-mm) ductile crack extension and recognizes the possibility for metal cleavage and brittle fracture at some upper shelf temperatures.

- Initial observation of a difference in radiation effect on the J_{Ic} value and the tearing modulus of A533-B steel. (A 10% reduction in J_{Ic} versus a 50% reduction in the tearing modulus was found in one irradiation test.) This difference was determined using the single-specimen compliance technique.

INTRODUCTION

J. R. Hawthorne

The cooperative research and development program between the Electric Power Research Institute (EPRI) and the Naval Research Laboratory (NRL) is generally directed at materials and material applications for nuclear energy systems, with research emphasis on material reliability and environmental responses for system safety. The present effort focuses on the degradation of fracture resistance of reactor vessel steels and weld metals by the 288°C (550°F) radiation environment. Properties under study are notch ductility, fracture toughness, and strength. Objectives are (a) to develop a data base for the evaluation of current radiation-embrittlement projection methods and for the development of improved procedures, (b) to investigate the relationship, if one exists, between radiation effects measured by the C_v test method and fracture mechanics test methods, (c) to determine the radiation embrittlement sensitivities of a broad range of reactor pressure vessel materials (plates, forgings, welds), and (d) to experimentally assess the effects of selected composition variations.

This report summarizes achievements of the second year of program effort. A previous report [1] described program progress in CY 1977, which focused on project design, materials selection, acquisition and development of the reactor experiment irradiation facility, initial irradiation operations, and planning for postirradiation testing and analysis. Plans and objectives for program research during CY 1979 are also outlined.

MATERIALS

J. R. Hawthorne

Material Selection

The selection of materials to meet program objectives was accomplished jointly by NRL and EPRI. To review [1], eight materials were chosen for investigation and are listed in Table 1. The three plates and the forging were selected from those commercial materials evaluated in the unirradiated condition by EPRI Program RP232. The A533-B steel plates, codes CAB and CBB, additionally were chosen to compare U.S. and European steel production. The third plate, code N, is known as the ASTM A302-B reference correlation monitor material and has seen wide use in reactor vessel surveillance programs [2]. Unlike the plate and forging materials, desired weldment materials were unavailable and had to be

specially fabricated for the program. As noted in Table 1, the four welds permit an assessment of the detrimental effect on radiation resistance of two levels of impurity copper content (≈0.35% Cu (high) and ≈0.20% Cu (intermediate)) and also assessment of the significance to postirradiation upper shelf energy (USE) retention of two welding flux types. Flux type 1 (Linde 80) typically produces a C_v upper shelf energy level that is relatively low (81 to 95 J); flux type 2 (Linde 0091 or Linde 124) typically produces a C_v upper shelf level that is high (>122 J). Both types have been applied extensively in reactor vessel fabrication.

Table 1 — Program Materials

Material	Code	Type
A533-B plate	CAB	U.S. production
A533-B plate	CBB	Foreign production
A302-B plate	N	U.S. production (ASTM A302-B reference)
A508-2 forging	BCB	U.S. production
S/A* weld 1	E19	High copper content (≈0.35% Cu) and low upper shelf energy (USE)
S/A weld 2	E24	High copper content and high USE
S/A weld 3	E23	Intermediate copper content (≈0.20% Cu) and low USE
S/A weld 4	E4	Intermediate copper content and high USE

*Submerged arc weld process.

Test Matrix

The irradiation test matrix is summarized in Table 2. Each of the 12 experiments include standard C_v specimens for notch ductility determinations and PCC_v and fatigue precracked 2.54-cm (1-in.) CT specimens for fracture toughness determinations. The three fluence levels respectively represent initial reactor vessel service, early vessel life, and end-of-life conditions. The intermediate fluence condition, $\approx 8 \times 10^{18}$ n/cm^2, is of special interest because it corresponds closely to the knee of the trend curve of radiation-induced transition temperature elevation versus fluence exhibited by the ASTM A302-B reference plate [2] and other pressure vessel materials.

Table 2 — Irradiation Test Matrix

Material*	Irradiation Assessments		
	1-2 X 10^{18} n/cm^2 > 1 MeV	≈8 X 10^{18} n/cm^2 > 1 MeV	3-4 X 10^{19} n/cm^2 > 1 MeV
A533-B plate (CAB)		• (BSR-2)*	• (BSR-3,5)
A533-B plate (CBB)			• (BSR-4)
A302-B plate (N)			• (BSR-7)
A508-2 forging (BCB)			• (BSR-6)
Weld 1 (E19)	• (BSR-9)	• (BSR-8)	• (BSR-10)
Weld 2 (E24)		• (BSR-11)	
Weld 3 (E23)		• (BSR-12)	
Weld 4 (E4)			• (BSR-13)

*Bulk Shielding Reactor, experiment 2.

† The material for experiment 12 (BSR-14) is not yet designated.

Material Procurement and Specimen Cutting

In CY 1977 the three plates and the forging were received at NRL from the EPRI Program RP232 archives. During the past year the four weldments were delivered to NRL to complete the required inventory of materials.

Specimen cutting, machining, and fatigue precracking were completed for the plates, the forging, and weldment E19 in CY 1978. Specimen fabrication was also undertaken for weldments E23 and E24. Required specimens of these weldments and weldment E4 will be available by 15 April 1979. An NRL Memorandum Report detailing specimen cutting and fabrication for individual materials is in preparation. For thermal control tests, final specimen machining and fatigue precracking, where required, will take place after specimen thermal conditioning.

The C_v and PCC_v specimens were machined to the standard dimensions given by ASTM Recommended Practice E23 (type A specimens). The CT specimens were machined to the dimensions given in Fig. 1 [1]. Specifications for fatigue precracking of PCC_v and CT specimens provided an a/W ratio of 0.5. The maximum allowable stress intensity (K_I) during the last increment of fatigue crack growth, 0.76 mm (0.030 in.), was 138 MPa$\sqrt{m}$ (20 ksi$\sqrt{in.}$) and 152 MPa$\sqrt{m}$ (22 ksi$\sqrt{in.}$) for the PCC_v and CT specimens respectively. Specimen fatigue precracking records document fatigue cycles, stress intensity, R ratio, and surface crack lengths for all stages of precracking.

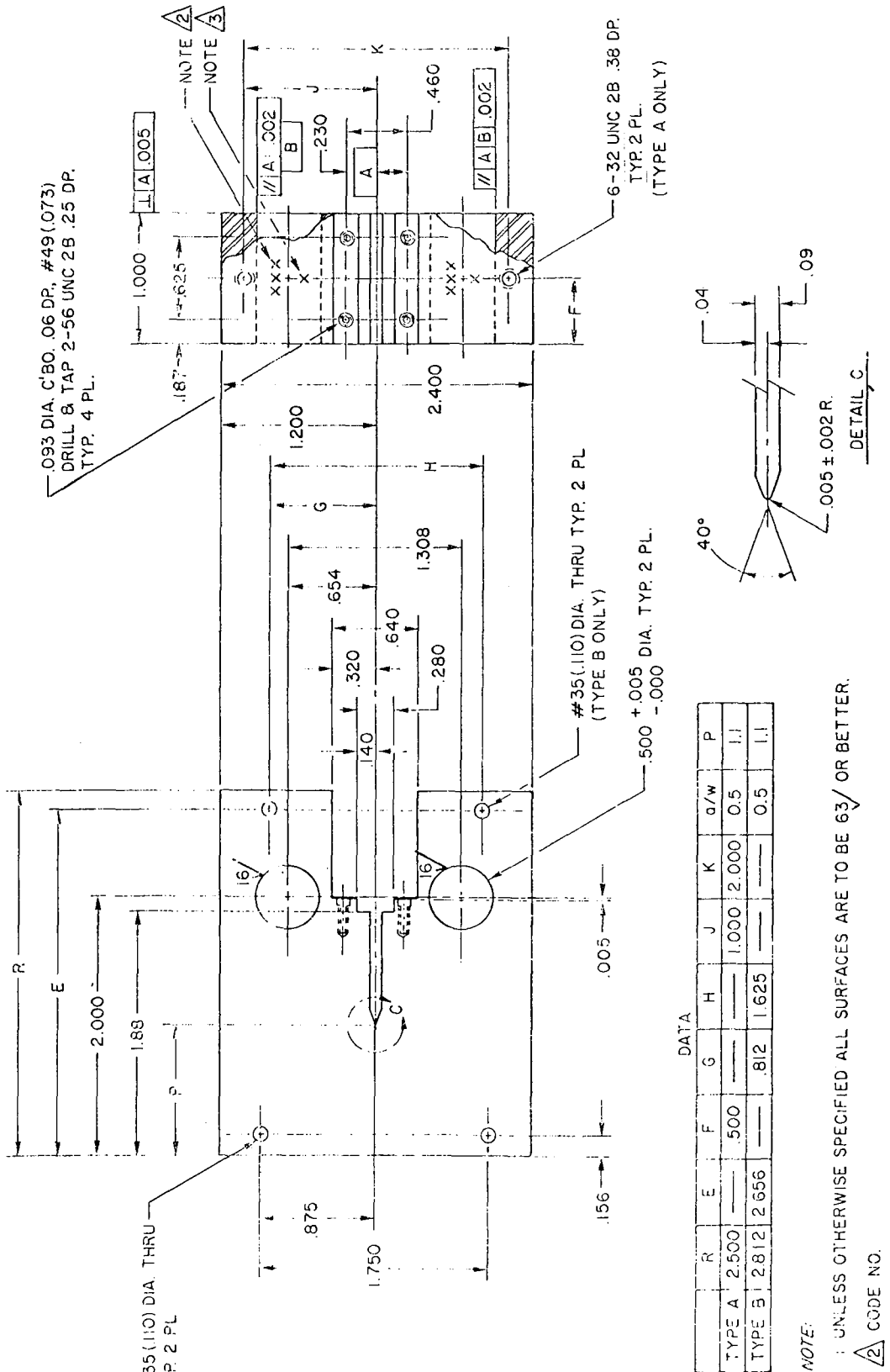

DATA

	R	E	F	G	H	J	K	a/w	P
TYPE A	2.500	—	.500	—	—	1.000	2.000	0.5	1.1
TYPE B	2.812	2.656	—	.812	1.625	—	—	0.5	1.1

NOTE:

1. UNLESS OTHERWISE SPECIFIED ALL SURFACES ARE TO BE 63 OR BETTER.
2. CODE NO.
3. CONSECUTIVE NO.

Fig. 1 — Design of the compact toughness (CT) specimen. (The dimensions are in inches; they can be converted to millimeters by multiplying by 25.4.)

REACTOR FACILITY AND OPERATIONS

H. E. Watson and J. R. Hawthorne

Reactor Facility

The test reactor facility employed for program irradiations is the Bulk Shielding Reactor (BSR) at the Oak Ridge National Laboratory (ORNL). Events leading to the selection of the BSR were described earlier [1].

In CY 1978 the experiment irradiation capabilities at the BSR were upgraded to permit the irradiation of two experiments simultaneously. This involved expanding the experiment control console to accommodate both experiments, installing a duplicate experiment instrumentation and piping system between the control console and the reactor bridge, and constructing a second reactor safety circuit system. Simultaneous irradiation operations commenced on 29 June 1978.

Irradiation Operations

For simultaneous experiment operations the BSR staff selected fuel core position 78 for the second irradiation facility (Fig. 2a). Fuel core position 67, the facility used initially, would be retained under this plan. A major, unexpected problem was encountered with the new core arrangement, however, which took several weeks to resolve satisfactorily. In brief, the insertion of an experiment in the new (second) facility severely affected the temperature uniformity and control of experiments in the original facility. The interference ultimately was isolated with two specially constructed, dummy experiments. The use of positions 76 and 78 subsequently was requested with the aim of obtaining experiment separation and a better balance within the core (Fig. 2b). Tests of this second core configuration, using the dummy experiments, showed much improved temperature uniformity but somewhat excessive (10 to 15%) gamma heating. The substitution of a solid aluminum piece for the fuel element between the experiment positions corrected this problem (Fig. 2c).

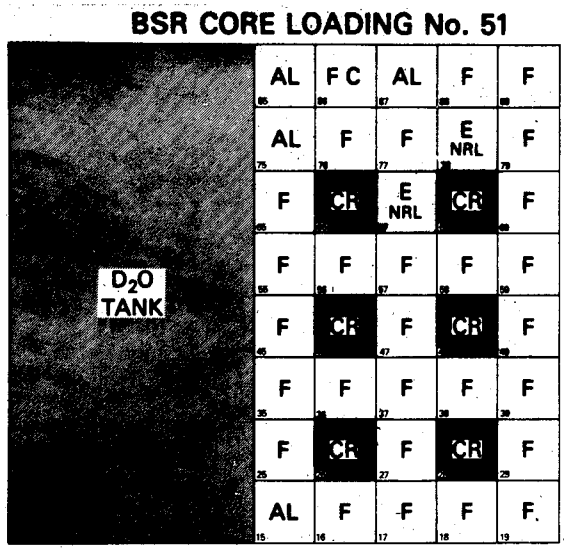

Fig. 2a — Fuel core configuration in the BSR reactor showing the first NRL-EPRI experiment irradiation facility (position 67) and the initially proposed second irradiation facility (position 78). The designations F, CR, FC, and AL stand respectively for fuel element, control rod, fission chamber, and aluminum piece

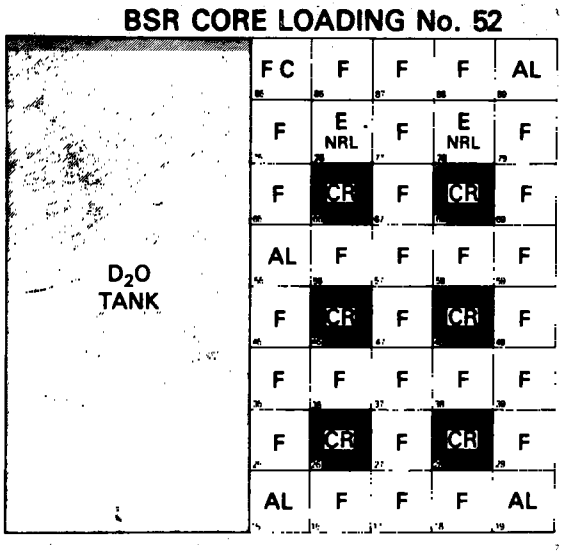

Fig. 2b — Fuel core configuration in the BSR reactor showing the two irradiation facilities (positions 76 and 78) subsequently requested by NRL for simultaneous experiment operations

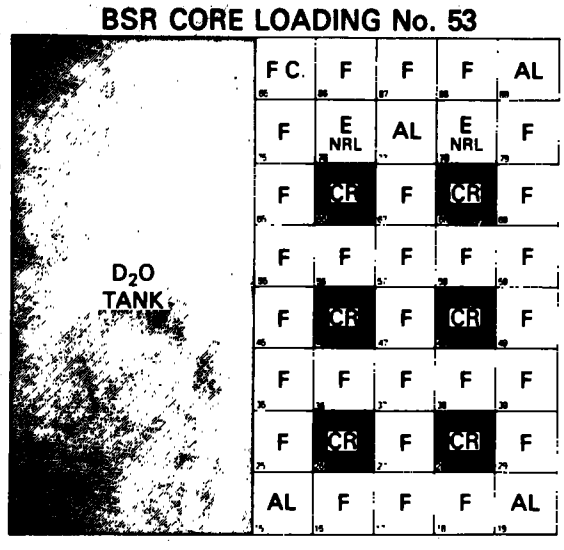

Fig. 2c — Final fuel core configuration in the BSR reactor for simultaneous NRL-EPRI experiment operations

Operations have indicated both experiments to be very sensitive to small reactor core changes. This is caused by the small pressure drop across the core and the resulting low reactor-coolant flow past the experiments. Low flow characteristics also necessitated the use of an elaborate reactor safety system to protect against experiment overheating. Four individual safety circuits are required by the BSR for each experiment (two per subsection). Because the NRL console has a built-in system to handle experiment overheat situations, the two safety circuits represent redundant, backup systems.

Neutron Flux Surveys

Surveys of ambient neutron flux conditions in positions 76 and 78 were performed to determine the flux gradients (axial and radial) in each of the facilities and to verify reactor-staff projections of ambient flux levels (n/cm^2 > 1 MeV). The design of the flux monitor assembly is shown in Fig. 3. Longitudinal holes over the assembly length received sealed aluminum tubes containing Fe and Ni flux monitor wires. (CoAl and AgAl flux monitor wires as well as Fe and Ni flux monitor wires are normally included in each material irradiation experiment.) During the exposure of the assembly, a dummy material-irradiation experiment was placed in the other position for better approximation of the normal core loading condition. The design of the assembly differs from that used previously for the survey of position 67 [1]; that is, the present design features a uniform metal density over the greater portion of its length to produce a more accurate measurement of the axial flux gradient. The greater relative mass of the assembly was expected to produce only a minor flux suppression.

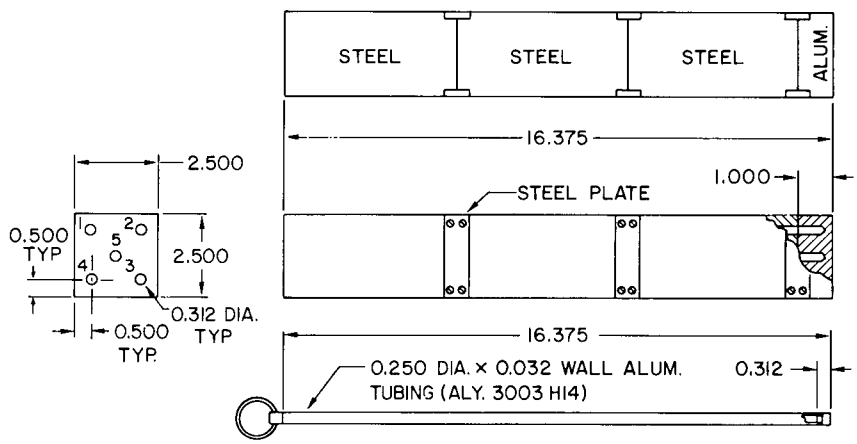

Fig. 3 — Experimental assembly used for neutron flux surveys in the NRL-EPRI irradiation facilities in the BSR reactor (core positions 76 and 78). (The dimensions are in inches.)

Each flux survey irradiation involved a 44,055-kilowatt-hour exposure. Monitor wires were analyzed at the Radiation Counting Laboratory of EG&G Idaho, Inc. Individual determinations are listed in Tables 3a and 3b. Neutron flux levels and gradients in the facilities are illustrated in Figs. 4a and 4b. Results obtained earlier for position 67 [1] are given in Fig. 4c. Three general observations are made: measured flux levels in positions 76 and 78 are considerably lower than that in position 67, requiring longer exposure times to obtain specific (target) fluences; flux levels in both positions 76 and 78 are of about the same magnitude; and radial flux gradients in positions 76 and 78 are less than the gradient in position 67. In spite of the reduced radial gradients, the practice of rotating experiments 180° at midcycle to balance the neutron exposures over the experiment cross section will be continued.

Table 3a — Results of NRL Neutron Flux Survey of BSR Experiment Facility 76

Monitor Test Position	Elevation		Flux $\emptyset$ (10^{12} n/cm^2·s > 1 MeV)							
			Tube 1		Tube 2		Tube 3	Tube 4	Tube 5	
	mm	in.	Fe*	Ni†	Fe	Ni	Fe	Fe	Fe	Ni
1	411	16.2	3.39	3.45	3.30	3.44	4.41	4.13	3.27	3.32
2	386	15.2	3.54	3.70	3.46	3.63	4.63	4.59	3.46	3.56
3	361	14.2	3.80	3.86	3.60	4.01	4.81	4.75	3.66	3.75
4	335	13.2	3.96	4.05	3.75	4.03	5.11	4.93	3.74	3.90
5	297	11.7	4.10	4.22	3.89	4.09	5.26	5.16	3.95	4.04
6	259	10.2	4.20	4.29	4.03	4.18	5.43	5.27	3.96	4.19
7	221	8.7	4.19	4.43	4.03	4.26	5.48	5.26	4.05	4.18
8	183	7.2	4.08	4.28	3.93	4.04	5.34	5.11	3.91	4.04
9	145	5.7	3.93	4.12	3.74	3.93	5.14	4.98	3.73	3.91
10	119	4.7	3.69	3.83	3.62	3.69	4.96	4.69	3.58	3.63
11	94	3.7	3.42	3.64	3.35	3.54	4.54	4.32	3.31	3.46
12	69	2.7	3.16	3.29	3.07	3.25	4.28	3.94	3.07	3.16
13	43	1.7	2.88	3.01	2.77	2.94	3.90	3.55	2.84	2.85

*^{54}Fe$(n,p)^{54}$Mn reaction.

†^{58}Ni$(n,p)^{58}$Co reaction.

Table 3b — Results of NRL Neutron Flux Survey of BSR Experiment Facility 78

Monitor Test Position	Elevation		Flux $\emptyset$ (10^{12} n/cm^2·s > 1 MeV)							
			Tube 1	Tube 2		Tube 3	Tube 4		Tube 5	
	mm	in.	Fe	Fe	Ni	Fe	Fe	Ni	Fe	Ni
1	411	16.2	3.07	2.99	3.05	4.11	3.73	3.80	3.11	3.13
2	386	15.2	3.22	3.21	3.26	4.32	4.05	4.10	3.27	3.47
3	361	14.2	3.45	3.38	3.40	4.54	4.35	4.45	3.41	3.54
4	335	13.2	3.53	3.51	3.63	4.79	4.55	4.70	3.60	3.70
5	297	11.7	3.70	3.74	3.85	5.01	4.79	4.86	3.75	3.94
6	259	10.2	3.74	3.82	3.94	5.19	4.99	4.96	3.87	4.14
7	221	8.7	3.78	3.83	3.98	5.14	5.03	5.08	3.91	4.08
8	183	7.2	3.70	3.76	3.97	5.07	4.92	5.06	3.91	4.00
9	145	5.7	3.56	3.69	3.73	4.79	4.64	4.88	3.69	3.93
10	119	4.7	3.49	3.55	3.55	4.66	4.33	4.69	3.59	3.70
11	94	3.7	3.21	3.25	3.34	4.30	4.22	4.37	3.35	3.50
12	69	2.7	2.98	3.09	3.14	4.01	3.83	3.98	3.09	3.21
13	43	1.7	2.73	2.78	2.92	3.77	3.61	3.66	2.90	2.99

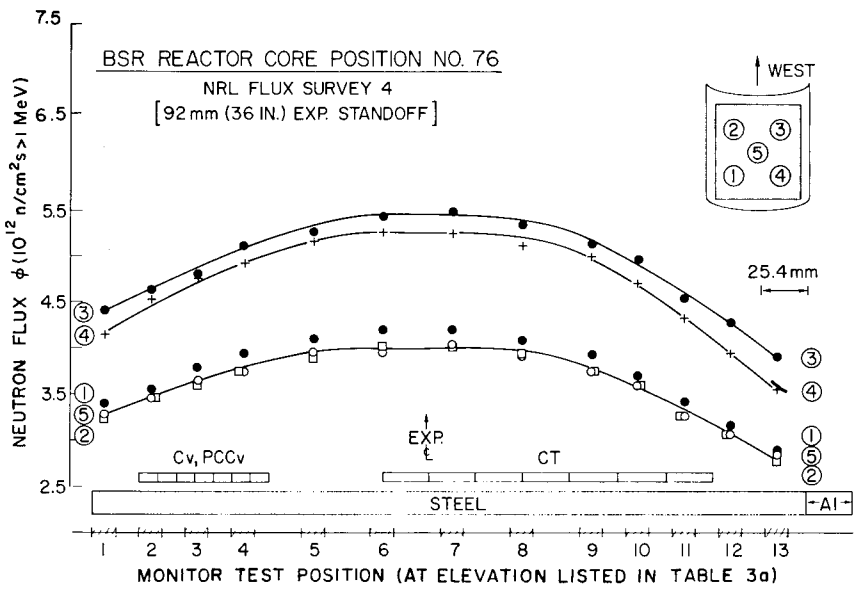

Fig. 4a — Results of an NRL neutron flux survey in BSR reactor core position 76 (BSR core loading 53). (The approximate elevations of test specimens in the core piece are also shown.)

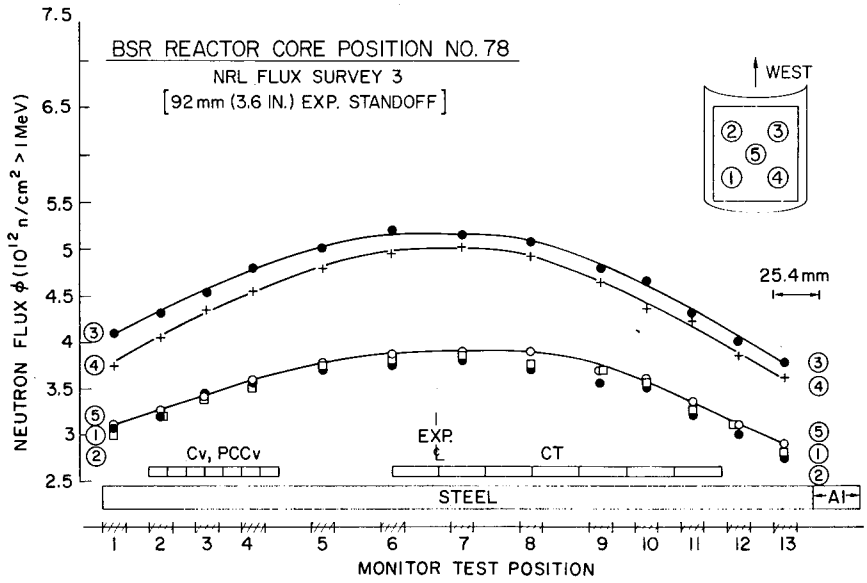

Fig. 4b — Results of an NRL neutron flux survey of BSR reactor core position 78 (BSR core loading 53)

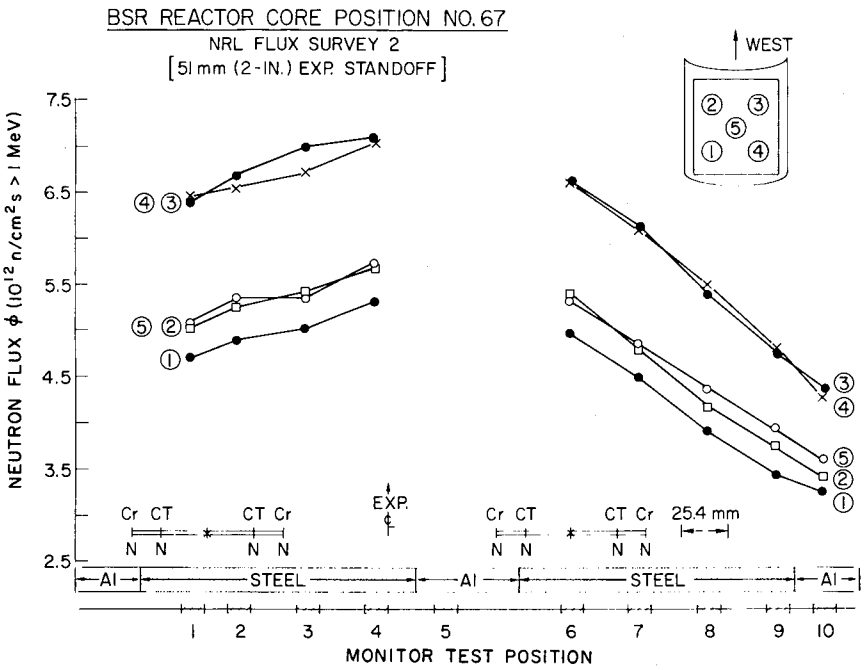

Fig. 4c — Results of an NRL neutron flux survey of BSR reactor core position 67 (BSR core loading 46)

Experiment Design

Preceding the conversion to simultaneous irradiation operations, a change was made in the experiment design. Figure 5 schematically illustrates the new and old design. The design change was part of the continuing effort to improve overall exposure conditions. Benefits are:

- Reduced specimen-to-specimen temperature differences. (The specimen group within each assembly now approaches a solid mass with shortened heat transfer paths.)

- Commingled C_v and PCC_v specimens. (The procedure minimizes fluence and temperature differences and improves the basis for a direct comparison of results.)

- Improved orientation of the CT specimen crack plane relative to the incident neutron flux.

- Reduced overall assembly length.

- Simplified experiment midcycle rotation.

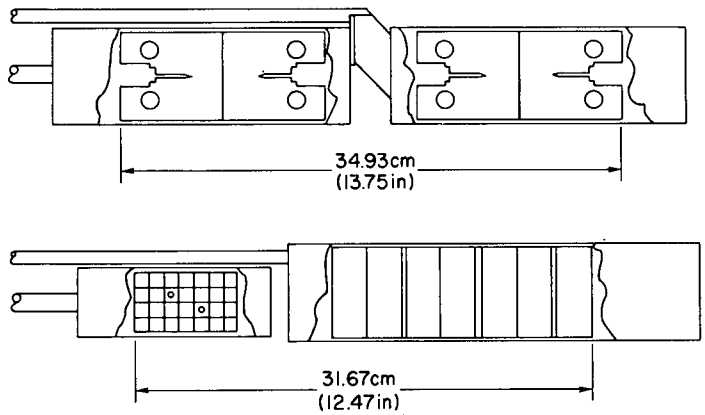

Fig. 5 — Elevation view showing the general design of the new material-irradiation assembly (bottom) and the old (initial) irradiation assembly (top)

Status of Material Irradiation

Figure 6a shows the experiment irradiation schedule for CY 1978, and Fig. 6b shows the schedule projected for CY 1979. It is expected that the schedule for CY 1979 will need periodic revision to take into account reactor outages for unscheduled maintenance, unexpected ORNL experiment operations, and refueling. In recognition of the required extension of experiment irradiation times due to lower flux levels and current projections

of unscheduled reactor outages, a 4-month extension of the program timeframe has been granted by the sponsor. Accordingly, the date for completion of phase 1 efforts has been advanced to 10 May 1980, even though, as shown in Fig. 6b, the current plan is to execute the experiment irradiations by August 1979.

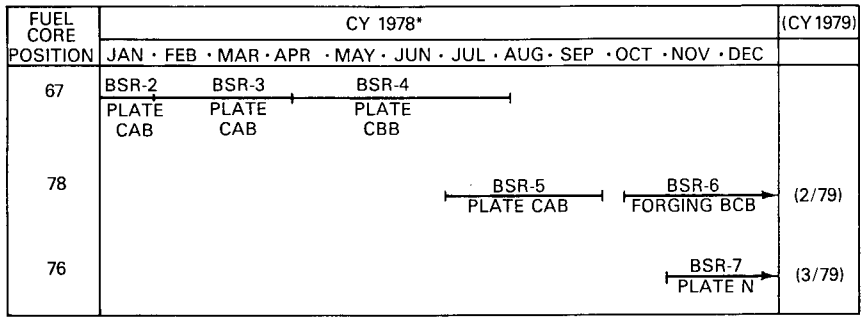

*FLUX SURVEY EXPERIMENTS 2, 3 AND 4 ARE NOT SHOWN

Fig. 6a — Experiment irradiation schedule for CY 1978

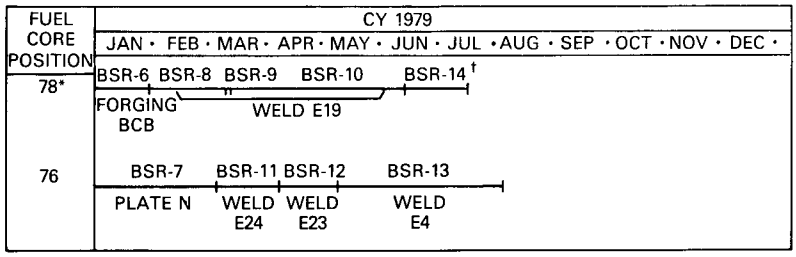

*SCHEDULE TO BE INTERRUPTED FOR SPECIAL ANL FLUX MONITOR EXPERIMENT
†MATERIAL NOT SELECTED

Fig 6b — Experiment irradiation schedule projected for CY 1979

FRACTURE TOUGHNESS TESTING

Overview

J. R. Hawthorne

Major research emphasis is on the definition of toughness trends relative to the brittle-to-ductile transition regime as functions of fluence level, product form, chemical composition, and test method. The program permits limited studies of the upper shelf, however, as specimen numbers permit. To evolve a full analysis of data significance, irradiation data and trend information developed by the present program will be evaluated statistically by a related EPRI program.

In CY 1978 the test plan for postirradiation PCC_V specimen evaluations was developed. Plans for postirradiation evaluations of C_V and CT specimens were developed in CY 1977 and are described in Ref. 1. The PCC_V test plan, outlined in Table 4, references specimen test temperatures to the estimated postirradiation nil-ductility transition (NDT) temperature. The postirradiation NDT temperature is estimated by adding the measured elevation in C_V 41-J (30 ft-lb) transition temperature to the measured NDT temperature (drop-weight test) for the preirradiation condition.

Table 4 — Plan for Postirradiation PCC_V Specimen Tests

Test Sequence	Specimen Test Temperature	
	High USE Materials	Low USE Materials
1	NDT + 60°F (33°C)	NDT + 60°F (33°C)
2	NDT	NDT + 120°F (67°C)
3	NDT + 120°F (67°C)	NDT + 90°F (50°C)
4	NDT + 90°F (50°C)	NDT
5	NDT + 60°F (33°C)	NDT + 60°F (33°C)
Data review and decision point		
6	NDT + 30°F (17°C)	NDT + 30°F (17°C)
7	NDT + 150°F (83°C)	NDT + 150°F (83°C)
8	NDT + 110°F (61°C) (option)	NDT - 60°F (33°C) (option)
9	NDT - 60°F (33°C) (option)	Upper shelf (option)
10	Upper shelf (option)	Upper shelf (option)

The PCC_V and C_V specimens are being tested in the dynamic mode; the CT specimens are being tested in the static mode. Specimen evaluations are proceeding in the order C_V, PCC_V, and finally CT. The test temperature range for each specimen type is an independent variable. A prerequisite to postirradiation evaluations is an availability of baseline data for the preirradiation condition.

Charpy-V (C_V) and Precracked Charpy-V (PCC_V) Specimen Evaluations

J. R. Hawthorne

Unirradiated Condition

Data for the unirradiated condition of the plate and forging materials have been reported by the EPRI RP232 Program [3-5]. Nonetheless, limited C_V and PCC_V evaluations of this condition are being performed as a precaution to guard against possible property differences between the test sections used in the two programs. In the case of the newly fabricated weldments, NRL tests of the unirradiated condition will serve as the reference data base for its postirradiation comparisons. (Welds E19, E23, and E24 are also included in an EPRI-sponsored research program at Westinghouse.)

Figures 7a, 7b, and 7c compare C_v results obtained by NRL against data developed previously by the RP232 Program. With the forging, good agreement between NRL and RP232-Program determinations is found. With plate CAB, on the other hand, a difference in C_v 41-J transition temperature of about 22°C (40°F) is observed. In addition a difference in C_v upper shelf energy level of at least 54-J (40 ft-lb) is indicated. Significant differences between the respective data sets are also noted for plate CBB. The source of the variations has not been established; nevertheless the comparisons indicate the wisdom of performing routine check tests for a research program of this type. Possible causes of the property variations are an across-plate metallurgical variation or a difference in through-thickness testing location ($1/4T$ versus $3/4T$). Normal test-machine calibration is not a factor. The NRL impact test machines have been certified as to accuracy by the Army Materials and Mechanics Research Center (AMMRC) [6-9]. AMMRC standard calibration specimens, however, cover only the energy range below 115 J (85 ft-lb). Machine-to-machine differences above this energy range could conceivably still occur. With reference to the upper shelf results for plate CAB, an interchange of test specimens between NRL and Combustion Engineering, Inc., Windsor Laboratories, in the course of an earlier study [10] did show agreement of the machines within 4% tolerance at 190 J (140 ft-lb). (EPRI RP232 program C_v tests of plate CAB and CBB were conducted at Combustion Engineering, Inc., Chattanooga Laboratories.)

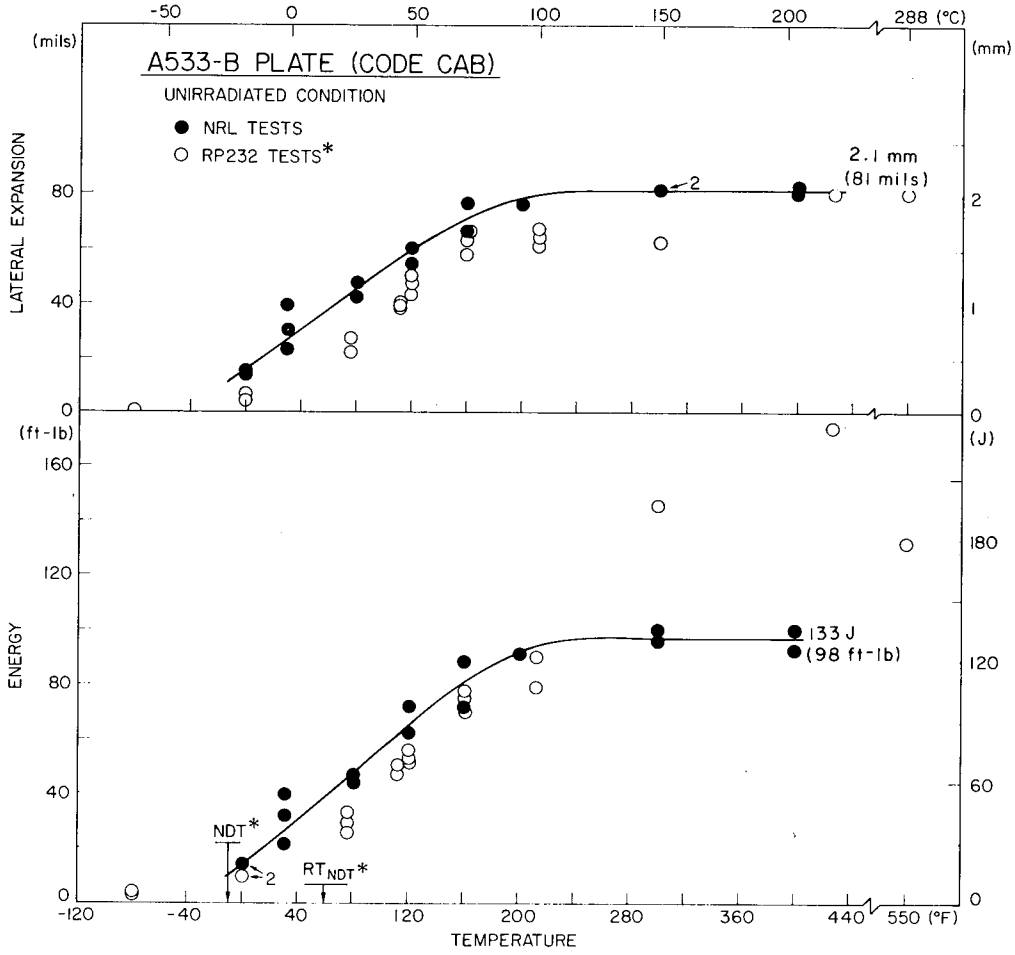

Fig. 7a — Charpy-V notch ductility of A533-B plate, code CAB, before irradiation. NRL test results and prior EPRI RP232 Program results are shown

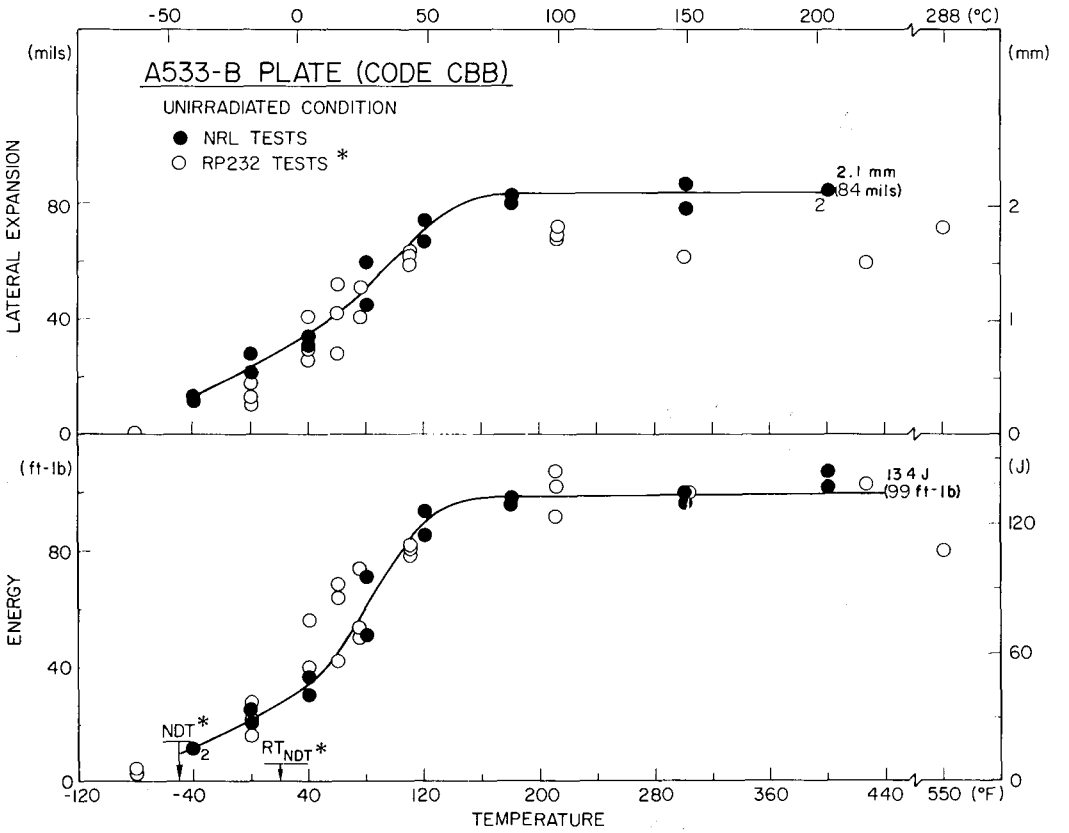

Fig. 7b — Charpy-V notch ductility of A533-B plate, code CAB, before irradiation

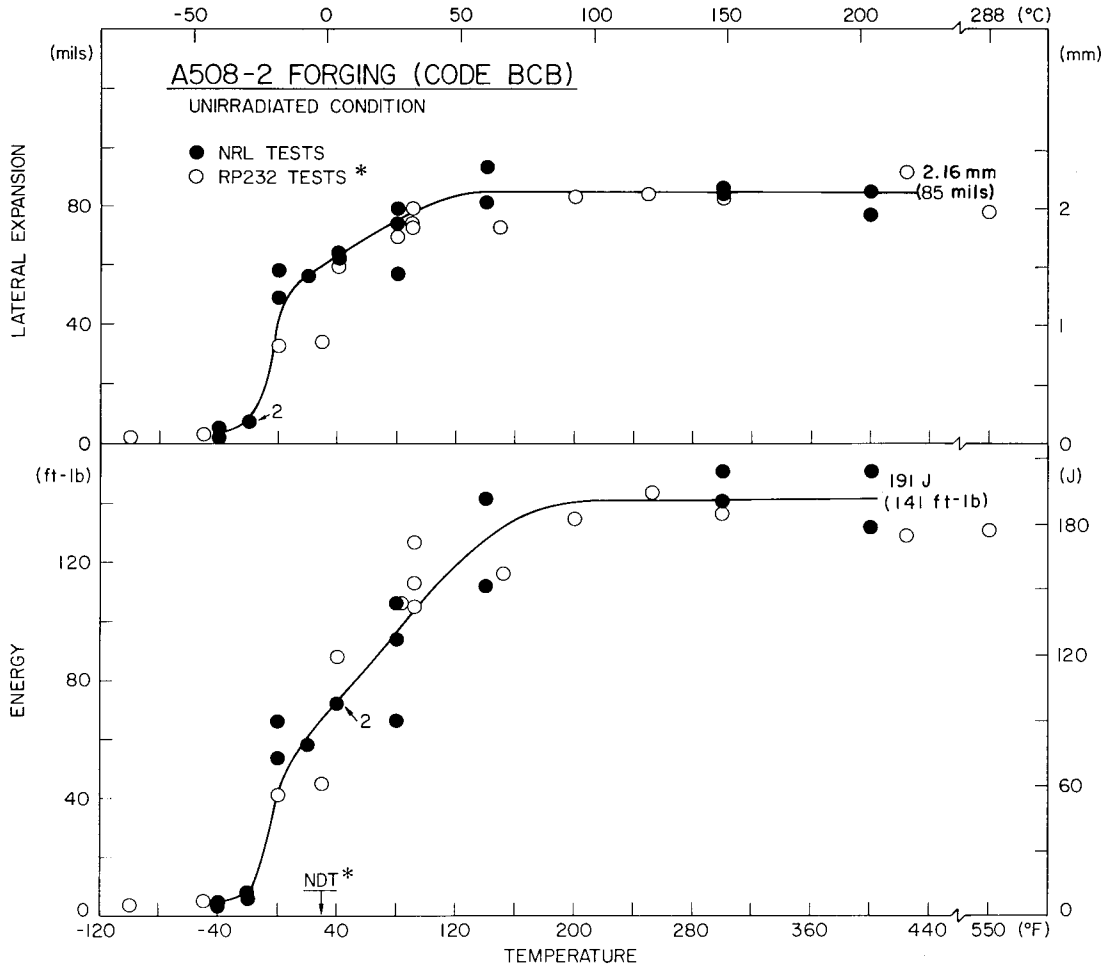

Fig. 7c — Charpy-V notch ductility of A508-2 forging, code BCB, before irradiation

Preirradiation-condition PCC_V tests of the plate and forging materials have not yet been accomplished. Accordingly irradiation data given in this report must reference PCC_V data from RP232 Program files.

Irradiated Condition

In CY 1978, postirradiation C_V tests were completed for the first four experiments (Table 2). Results for experiments BSR-2, BSR-3, and BSR-5, which contained plate CAB material, are presented in Figs. 8a, 8b, and 8c. Results for experiment BSR-4, which contained plate CBB material, are given in Fig. 8d. Table 5 summarizes the observed changes in notch ductility. The neutron fluence values in Fig. 8a are based on actual evaluations of neutron flux monitors contained in the experiment; values given in Fig. 8b, 8c, and 8d are preliminary estimates only. Also, experiments BSR-2 and BSR-3 were built to the initial irradiation assembly design, whereas experiments BSR-4 and BSR-5 were constructed to the currently used design (Fig. 5).

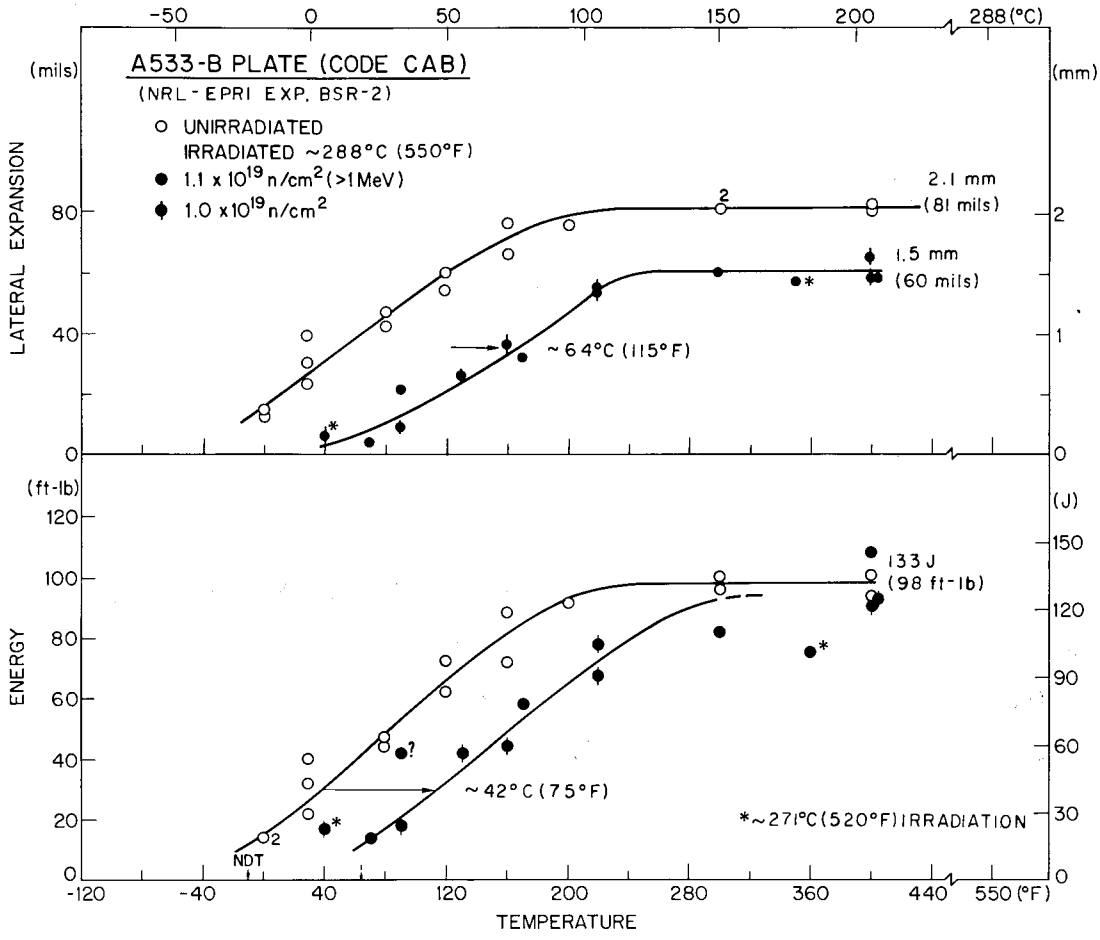

Fig. 8a — Charpy-V notch ductility of A533-B plate, code CAB, after irradiation (experiment BSR-2)

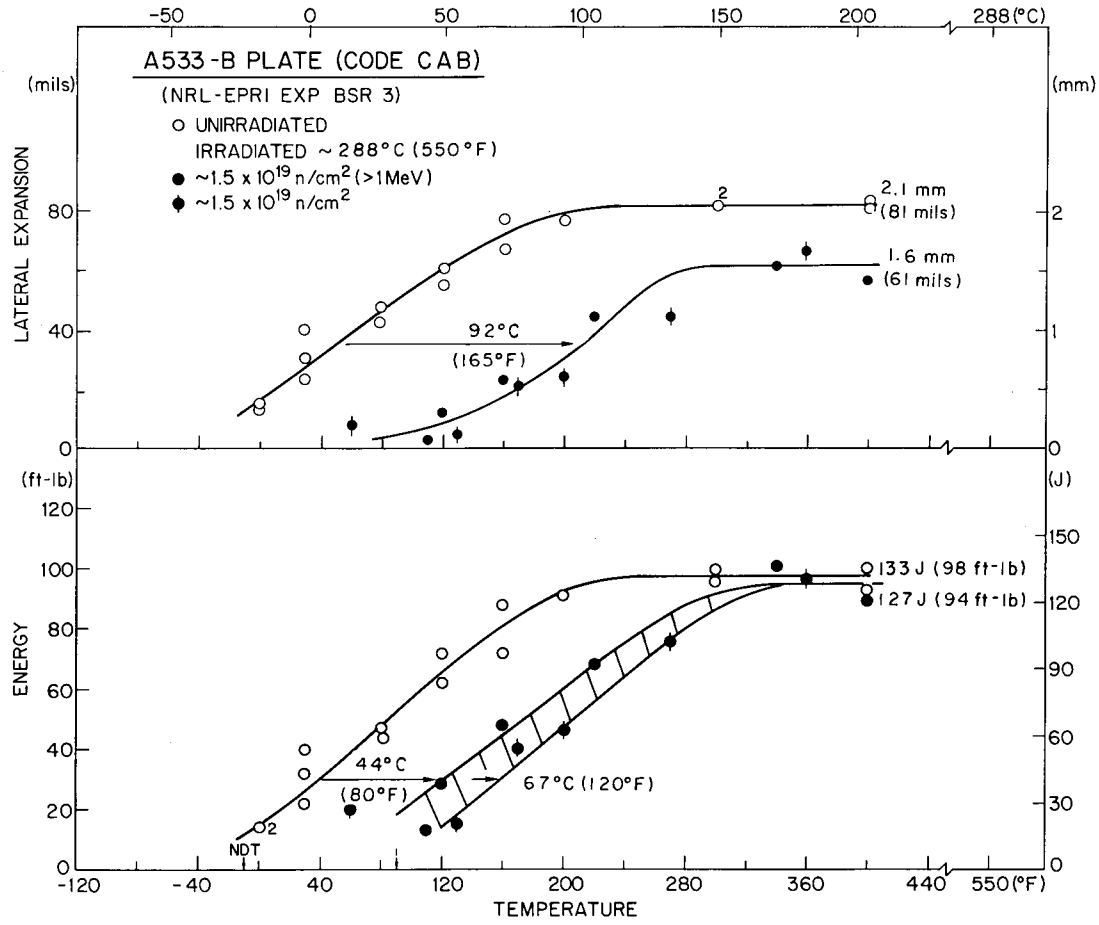

Fig. 8b — Charpy-V notch ductility of A533-B plate, code CAB, after irradiation (experiment BSR-3)

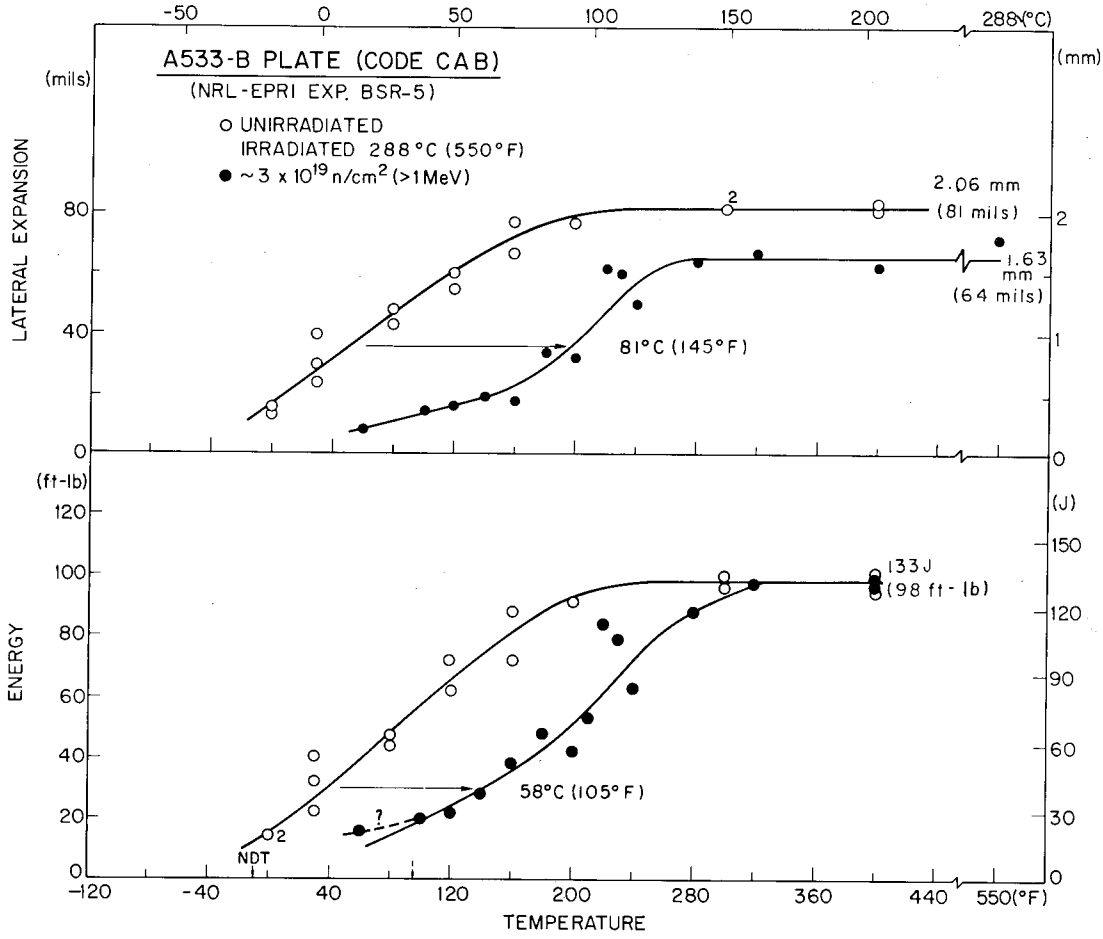

Fig. 8c — Charpy-V notch ductility of A533-B plate, code CAB, after irradiation (experiment BSR-5)

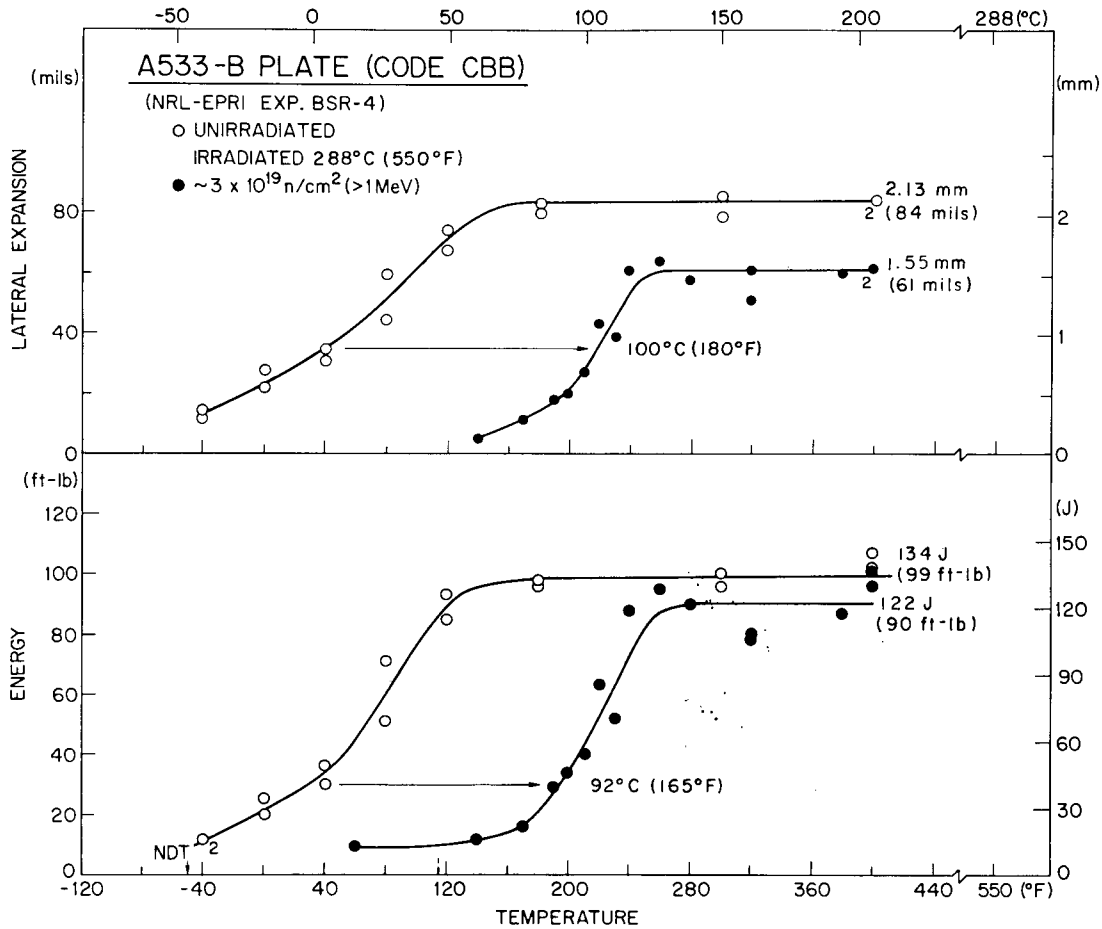

Fig. 8d — Charpy-V notch ductility of A533-B plate, code CBB, after irradiation (experiment BSR-4)

Table 5 — Postirradiation Charpy-V Properties as Shown in Figs. 8a Through 8d

Experiment	Fluence ϕ (10^{19} n/cm^2 >1 MeV)	C_V Transition Temperature						C_V Upper Shelf			
		41-J (30 ft-lb) Index		68-J (50 ft-lb) Index		0.9-mm (35-mil) Index		Energy		Lateral Expansion	
		°C	°F	°C	°F	°C	°F	J	ft-lb	mm	mils
Plate CAB											
—	Unirradiated	4	40	29	85	10	50	133	98	2.1	81
BSR-2	1.1	16	115	74	165	74	165	≈133	≈98	1.5	60
BSR-3	≈1.5*	≈60	≈140	≈88	≈190	102	215	≈127	≈94	1.6	61
BSR-5	≈3*	63	145	91	195	91	195	133	98	1.6	61
The preceding values indicate the following property changes (Δ) by irradiation											
BSR-2	1.1	42	75	41	80	61	115	<14	<10	0.5	21
BSR-3	≈1.5*	≈56	≈100	≈58	≈105	92	165	<14	<10	0.5	20
BSR-5	≈3*	58	105	61	110	81	145	≈ 0	≈ 0	0.1	17
Plate CBB											
	Unirradiated	-1	30	18	65	4	40	131	99	2.1	81
BSR-1	≈3*	91	195	101	220	101	220	≈122	≈90	1.6	61
The preceding values indicate the following property changes (Δ) by irradiation											
BSR-1	≈3*	92	165	86	155	100	180	<14	<10	0.6	24

*Preliminary fluence estimate.

Analyses of the C_v data permit several general observations:

- Good agreement is evident between the radiation-induced elevations in C_v 41-J and 68-J (30 ft-lb and 50 ft-lb) transition temperatures. On the other hand the elevation in the lateral-expansion 0.9-mm (35-mil) transition temperature generally is greater than the elevation in the 41-J transition temperature.

- The increases in the 41-J transition temperature measured for plate CAB (three experiments) were in the range of 42 and 58°C (75 to 105°F). The increase in the 41-J transition temperature for plate CBB was 92°C (165°F).

- Upper shelf reductions were uniformly 14 J (10 ft-lb) or less, indicating good upper shelf retention with irradiation. Lateral expansion values at upper shelf temperatures, in contrast, show greater reductions with irradiation.

An additional observation of special interest to the study is that the measured notch ductility changes in general are about equal to projections of radiation embrittlement given

by NRC Regulatory Guide 1.99 [11] for the individual steel chemistries and fluences. The expression offered by the Guide for calculation of transition temperature elevation by 288°C irradiation is

$$\Delta T\,(^{\circ}F) = [40 + 1000\,(\%Cu - 0.08) + 5000\,(\%P - 0.008)\,]\;(f/10^{19})^{1/2}, \qquad (1)$$

where f is fluence in $n/cm^2 > 1$ MeV. Table 6 compares calculated elevations in the C_v 41-J transition temperature and the measured elevations. For experiment BSR-5 the measured elevation in transition temperature is greater by 6°C (10°F), but this difference is not significant.

Table 6 — Comparison of Measured and Projected Elevations in the Charpy-V 41-J Transition Temperature by 288°C Irradiation

Material Code	Experiment	Fluence ϕ (10^{19} n/cm^2 > 1 MeV)	Elevation (°F)	
			Experiment Measurement	Reg. Guide 1.99 Projection (Eq. (1))
CAB (0.12% Cu, 0.008% P)	BSR-2	1.1	75	84
	BSR-3	1.5*	≈100†	98
	BSR-5	3.0*	105	139
CBB (0.13% Cu, 0.006% P)	BSR-4	3.0*	165	156

*Preliminary fluence estimate.
†Average value.

A further observation is that the data describe a higher radiation sensitivity for plate CBB than for plate CAB if preliminary fluence estimates are correct. The higher radiation sensitivity cannot be attributed to a difference in copper content or phosphorus content between the two plates (Table 7); on the other hand plate CBB is noted to have a much higher arsenic content than plate CAB. Previously [12] the question was raised as to a possible contribution of arsenic content to radiation sensitivity, because this impurity element and phosphorus have a similar influence with regard to steel temper embrittlement. Moreover the mechanism of the phosphorus contribution to radiation embrittlement is believed to be radiation-enhanced phosphorus diffusion to and weakening of ferrite/carbide interfaces. One study of the arsenic contribution, using NiCrMoV forging materials with yield strengths of about 724 MPa (105 ksi) and arsenic content variations between 10 and 170 ppm, has been reported [13]. No indication of an arsenic influence on radiation resistance was found; however, the arsenic content of plate CBB (350 ppm) in the present case is considerably higher than that range investigated.

Table 7 — Chemical Composition of Plates CAB and CBB [3] and Forging BCB [4]

Element	Chemical Composition (wt-%)		
	Plate CAB	Plate CBB	Forging BCB
C	0.25	0.21	0.212
Mn	1.41	1.45	0.63
P	0.008	0.006	0.006
S	0.014	0.009	0.012
Si	0.26	0.23	0.26
Ni	0.46	0.55	0.55
Cr	0.11	0.05	0.38
Mo	0.49	0.64	0.62
Al (soluble)	0.016	0.029	<0.001
Al (insoluble)	0.001	0.002	0.001*
As	0.012	0.035	0.004
B	0.0007	0.0004	<0.0002
Cb	<0.01	<0.01	<0.005
Co	0.010	0.020	<0.005
Cu	0.12	0.13	0.036
N	0.008	0.014	0.013
O	0.003	0.004	—
Pb	<0.001	<0.001	0.003
Sb	0.0013	0.0015	<0.004
Sn	0.008	0.015	0.011
Ti	<0.01	<0.01	<0.001
V	0.003	0.003	0.002
W	<0.01	<0.01	<0.012
Zr	<0.001	<0.001	<0.001

*Total aluminum.

In CY 1978, PCC_v tests were also completed for the first four irradiation experiments. The results are presented in Figs. 9a through 9d and summarized in Table 8. Postirradiation test procedures conformed to standard EPRI procedures for K_J determinations [14]. The present determinations were based on energy absorbed to maximum load corrected for specimen and test machine compliance.

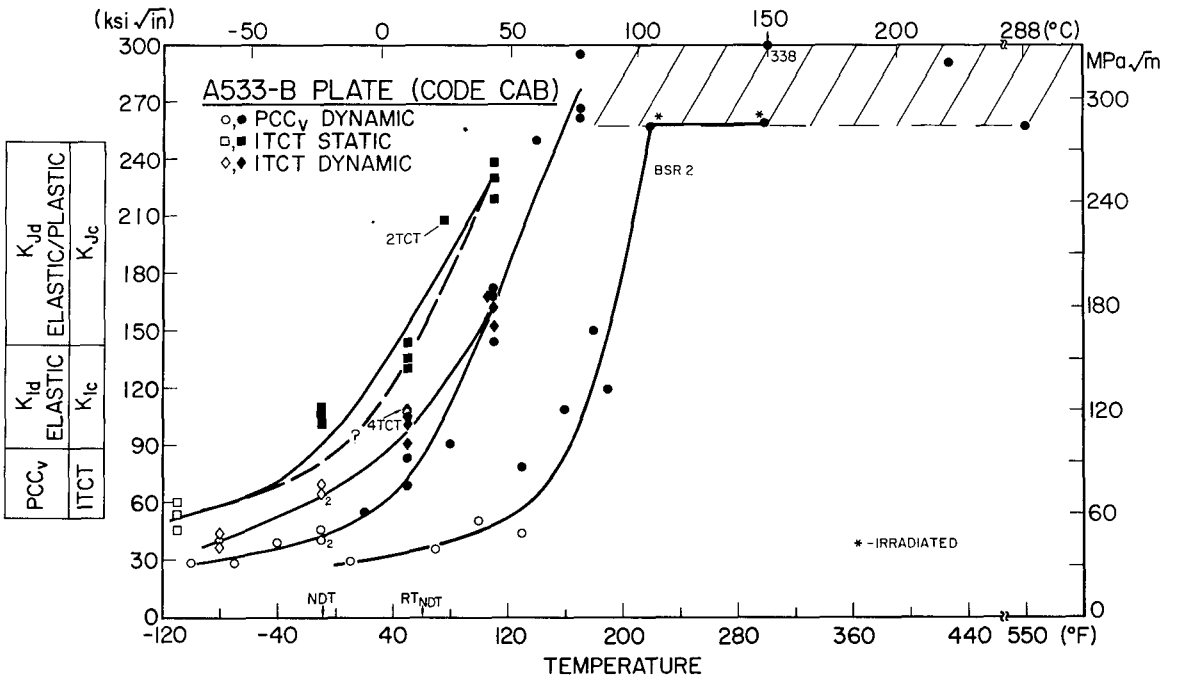

Fig. 9a — Fatigue precracked Charpy-V test results for A533-B plate, code CAB, before and after irradiation (experiment BSR-2). Compact toughness (CT) test results for the unirradiated condition developed by the EPRI RP232 program are also shown. (The nomenclature 1T-CT refers to toughness tests using a compact specimen 25.4 mm (1 in.) thick (Fig. 1). The nomenclature K_{Ic} and K_{Jc} are discussed in the next subsection.) The CT results have not been adjusted by the Merkle-Corten correction (to be discussed later) for the tension component of loading. The open symbols identify fractures before general yielding, and the filled symbols identify fractures after general yielding.

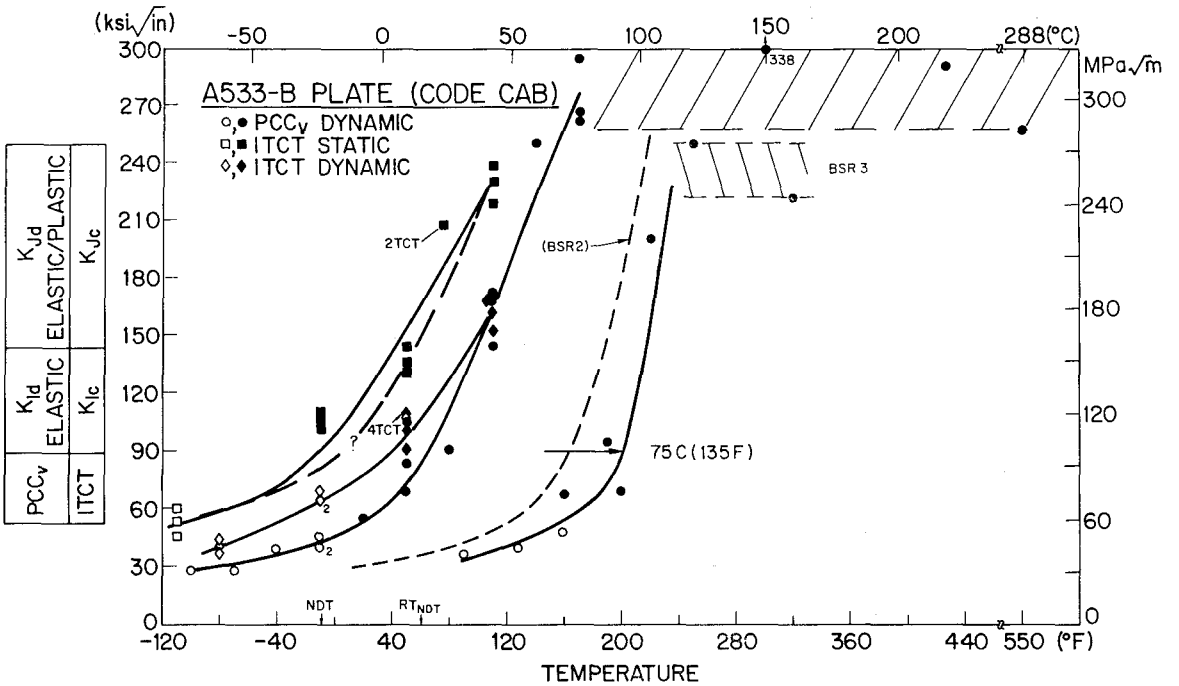

Fig. 9b — Fatigue precracked Charpy-V test results for A533-B plate, code CAB, before and after irradiation (experiment BSR-3)

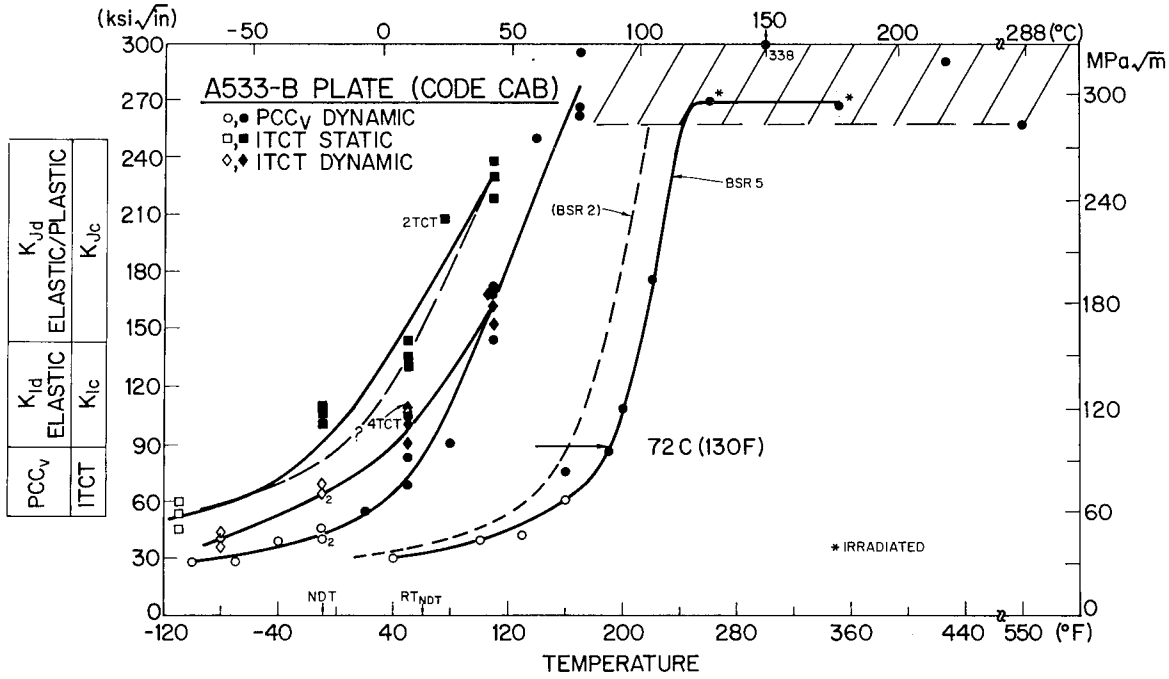

Fig. 9c — Fatigue precracked Charpy-V test results for A533-B plate, code CAB, before and after irradiation (experiment BSR-5)

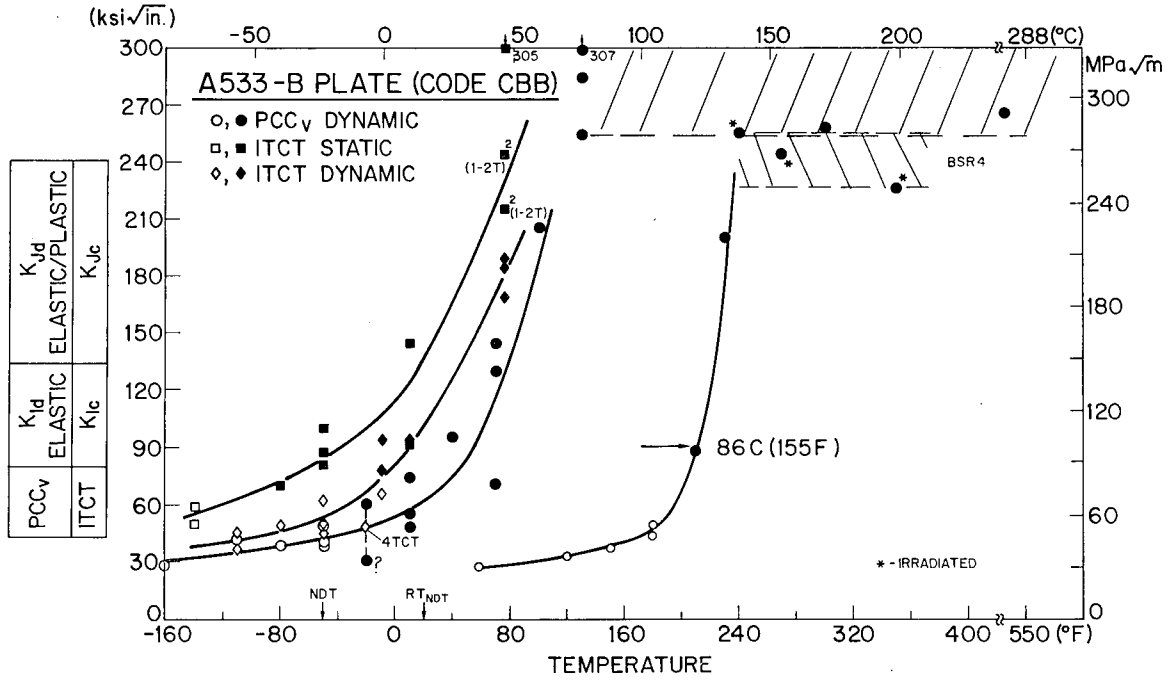

Fig. 9d — Fatigue precracked Charpy-V test results for A533-B plate, code CBB, before and after irradiation (experiment BSR-4)

Table 8 — Postirradiation Precracked Charpy-V Properties as shown in Figs. 9a through 9d

Experiment	Fluence ϕ (10^{19} n/cm^2 > 1 MeV)	K_{Jd} Transition Temperature						K_{Jd} Upper Shelf	
		99-MPa$\sqrt{m}$ Index		66-MPa$\sqrt{m}$ Index		132-MPa$\sqrt{m}$ Index			
		°C	°F	°C	°F	°C	°F	MPa$\sqrt{m}$	ksi$\sqrt{in.}$
Plate CAB									
—	Unirradiated	18	65	-1	30	29	85	>280	>255
BSR-2	1.1	77	170	57	135	85	185	286	260
BSR-3	≈1.5*	93	200	77	170	102	215	242-275	220-250
BSR-5	≈3*	91	195	71	160	99	210	291	265
The preceding values indicate the following property changes (Δ) by irradiation									
BSR-2	1.1	59	105	58	100	56	100	≈ 0	≈ 0
BSR-3	≈1.5*	75	135	78	140	73	130	≈22	≈20
BSR-5	≈3*	73	130	72	130	70	125	≈ 0	≈ 0
Plate CBB									
—	Unirradiated	13	55	9	15	21	70	285	260
BSR-4	≈3*	99	210	91	195	104	220	247-280	225-255
The preceding values indicate the following property changes (Δ) by irradiation									
BSR-1	≈3*	86	155	100	180	83	150	≈22	≈20

*Preliminary fluence estimate.
†Not clearly established.

Currently it is believed that the PCC_v specimen can define dynamic fracture toughness (K_{Jd}) in the transition region up to a value of approximately 110 MPa$\sqrt{m}$ (100 ksi$\sqrt{in.}$) using the *J*-integral calculation and the energy absorbed to maximum load. Because of possible crack extension prior to the maximum load, it is difficult to prove that values in excess of the preceding level can still be considered as "initiation" toughness. For post-irradiation comparisons the temperature corresponding to K_{Jd} = 99 MPa$\sqrt{m}$ (90 ksi$\sqrt{in.}$) was arbitrarily selected as an index of transition behavior. The PCC_v specimen is too small to measure a valid fracture toughness (ASTM E399 criteria for static tests) above a value of about 44 MPa$\sqrt{m}$ (40 ksi$\sqrt{in.}$). The specimen size and the *J*- integral procedure can be used to project K_{Jd} properties in excess of 44 MPa$\sqrt{m}$, but the method is considered fully acceptable only when fracture initiates in a cleavage mode.

Experimental observations from Figs. 9a through 9d and Table 8 are as follows:

- Good agreement is indicated between the radiation-induced elevations in K_{Jd} 99-, 66-, and 132-MPa$\sqrt{m}$ transition temperatures for plate CAB and for plate CBB.

- The elevations in the K_{Jd} 99-MPa$\sqrt{m}$ transition temperature for plate CAB (three experiments) range from 58 to 75°C (105 to 135°F). The elevation in the K_{Jd} 99-MPa$\sqrt{m}$ transition temperature for plate CBB is 86°C (155°F).

- The elevation in the K_{Jd} 99-MPa$\sqrt{m}$ transition temperature is slightly greater than the elevation in the C_v 41-J transition temperature for plate CAB but not for plate CBB.

- The PCC_v data trends support the C_v indications of a higher radiation sensitivity for plate CBB.

- Comparable radiation reductions in upper shelf fracture toughness are exhibited by plates CAB and CBB; postirradiation upper shelf values, however, exceed 165 MPa$\sqrt{m}$ (150 ksi$\sqrt{in.}$). PCC_v upper shelf reductions appear to be comparable to the C_v upper shelf energy reductions.

Relative to the third observation listed, the difference between PCC_v and C_v transition-temperature elevations may be the result of small fluence variations between specimen locations in the irradiation assembly or may reflect the use of RP232 Program data for the reference (unirradiated) condition. The use of RP232 Program data may also have a bearing on the last observation listed. NRL tests of the unirradiated condition should resolve this question.

To summarize PCC_v and C_v observations thus far, the data for transition-temperature elevation by irradiation appear to be internally consistent. The two plate materials evaluated demonstrate high upper shelf toughness retention but appear to differ in their resistance to radiation-induced transition temperature shift. The possibility that arsenic content contributes to radiation sensitivity at levels exceeding 120 ppm has been raised and bears further examination.

Development of *J-R* Curve Procedures

F. J. Loss, B. H. Menke, and R. A. Gray, Jr.

Focus

The primary focus of evaluations with the CT specimens is on fracture initiation toughness. However, it is expected that the materials will exhibit elastic-plastic behavior over the major portion of the brittle-to-ductile transition regime. Accordingly it becomes necessary to characterize the slow-stable crack extension phenomenon as commonly denoted by the *R* curve as well. The latter is useful not only in defining crack initiation but also in assessing the potential for crack instability.

The temperature shift ΔT between preirradiation and postirradiation K_{Ic}-versus-temperature curves developed by this study permits comparisons with analogous ΔT values measured from dynamic testing of C_v and PCC_v specimens. The development of such a correlation between the Charpy and fracture-mechanics test methods for the irradiated condition, if successful, will be of significant value in interpreting C_v results from reactor surveillance programs. The degradation in upper shelf toughness by irradiation, measured from the compact specimens, likewise will permit a comparison with postirradiation change in C_v upper shelf energy.

Approach

The 25.4-mm-thick (1-in.) CT specimen (1T-CT) (Fig. 1) was selected for preirradiation fracture toughness characterization because it can be irradiated easily and yet its relatively large size provides sufficient mechanical constraint to infer high levels of plane strain toughness when the specimen itself exhibits elastic-plastic behavior. By current J-based criteria, the 1T-CT specimen is believed to be large enough to permit characterization of the stable crack extension (R curve) to J values in excess of 600 kJ/m^2 (3430 lb/in.) for the types of steels considered here; an equivalent K_{Ic} in excess of 350 MPa$\sqrt{\text{m}}$ (320 ksi$\sqrt{\text{in.}}$) can also be determined. (A current thickness criteria for J_{Ic} testing requires the thickness B to be in excess of 25 J_{Ic}/σ_f, where σ_f is the mean stress between the yield stress and the ultimate stress.) Though initiation toughness levels of this magnitude are not necessarily required for reactor safety analysis, this specimen constraint capability is necessary for proper analysis of the R-curve behavior.

The 1T-CT specimen can measure a valid (E-399) K_{Ic} value no higher than approximately 60 MPa$\sqrt{\text{m}}$ (55 ksi$\sqrt{\text{in.}}$) for the irradiated steels in this program. Since most of the toughness values of practical interest lie above this value, plane strain (K_{Ic}) values must be inferred from elastic-plastic specimen behavior. The J-R curve approach is used whenever an E-399 K_{Ic} toughness cannot be defined. The inferred toughness, termed K_{Jc}, is computed from the well-known relation

$$K_{Jc} = \left(\frac{E J_{Ic}}{1 - \nu^2} \right)^{1/2}, \tag{2}$$

where J_{Ic} is the initiation toughness, E is Young's modulus, and ν is Poisson's ratio. The modulus is not measured independently but instead is taken from the relationship employed by Ireland and coworkers in an earlier EPRI-sponsored program [15]:

$$E = 30.2 - 0.0046\,T,$$

where E has the units of 10^6 psi and T is in degrees F. This becomes

$$E = 207{,}200 - 57.09T,$$

where E has the units megapascals and T is in degrees C.

Interpretation of J-Based Toughness

We have chosen to interpret K_{Jc} as the value of K_{Ic} which would have been obtained from a larger specimen meeting the E-399 size requirements. Unfortunately an unequivocal correspondence between K_{Jc} and K_{Ic} is not universally accepted. This correspondence is under investigation in a related program sponsored by EPRI. Also the value of K_{Jc} derived from the J_{Ic} value can be lower than a K_{Ic} value measured directly. This results from the ASTM E-399 definition of K_{Ic}, which has a built-in size effect. The latter arises from the permissible "apparent" crack extension of 2%. Clearly crack extensions of this magnitude can result in K_{Ic} values which correspond to different positions on a thickness-independent R curve. For large specimens this crack extension could result in an equivalent J value that is significantly above the initiation value J_{Ic}, depending on the slope of the R curve. Further interpretation of this behavior is beyond the scope of the current program.

A standard method for J_{Ic} measurement is being investigated by ASTM Committee E24.08 [16]. However, this proposed standard cannot be applied directly in the present program because J_{Ic} is defined by the multispecimen heat-tint technique, which is not employed here, and the standard does not provide a method for definition of the R curve. Proper definition of the R-curve trends is desirable, since the R curve can be used in conjunction with instability analysis of the structure by the tearing modulus (T) approach being developed by Paris and coworkers [17]. In addition, because of the limited number of specimens which can be irradiated and also because of the limited supply of the weld deposit material used in this program, it is essential that the J-R curve be defined by a single-specimen technique. In this investigation the single-specimen compliance (SSC) technique is being used exclusively [18].

The J_{Ic} level is derived from the intersection of the J-R curve with the formal crack-tip-blunting line, shown schematically in Fig. 10. The word formal is used because the blunting line defined in this manner may only approximate the actual behavior for a wide range of steels. Furthermore there is disagreement as to whether the slope of the R curve is specimen-thickness dependent even when a minimum thickness requirement has been met, such as $B > 25\ J/\sigma_f$. Fortunately it appears that the J_{Ic} value is independent of R-curve shape. However, an investigation of geometry dependence of the J-R curve is beyond the scope of the present program.

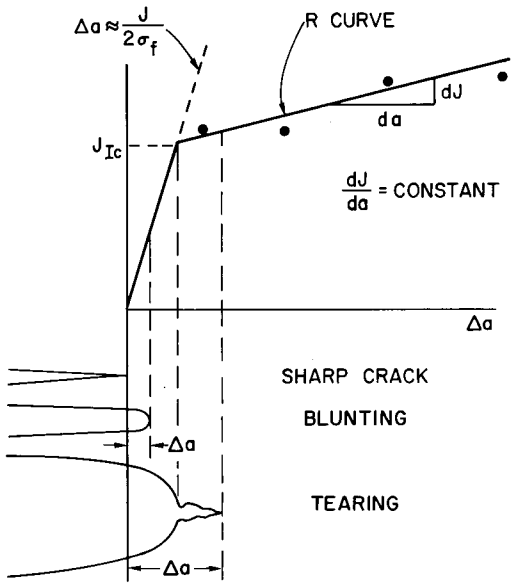

Fig. 10 — Definition of the J_{Ic} point as the intersection of the R curve with the crack-tip-blunting line

In this study the majority of the specimens are side grooved in order to provide a straight crack-front extension. This modification is believed to result in a J value which is nearly constant across the crack front [19]. A more constant J value, in turn, will define an R curve of lower slope than would have been obtained with smooth specimens, for those materials where the addition of grooves results in a tunneled crack front. It is believed that a conservative assessment of the stable crack extension will be obtained with the R curves of lower slope. Furthermore, if it can be shown that a plane-strain R curve is obtained with side-grooved specimens, then this behavior appears to be properly defined for use in studies of the structural response of flawed members under plane strain conditions.

Experimental Procedure

The SSC procedure has been employed by several laboratories in the United States to establish J_{Ic}. Only recently, however, has the method been extended to define the R curve. This procedure is simple in concept but requires highly accurate electronic and experimental apparatus for successful application. The primary goal in this method is to achieve a partial unloading of the specimen (say 10%) such that unload and reload records of load (P) vs deflection (δ) enable the specimen compliance (δ/P) to be determined with precision (Fig. 11, top). A predetermined compliance relationship (Fig. 11, bottom) is then used to establish the crack length with similar precision.

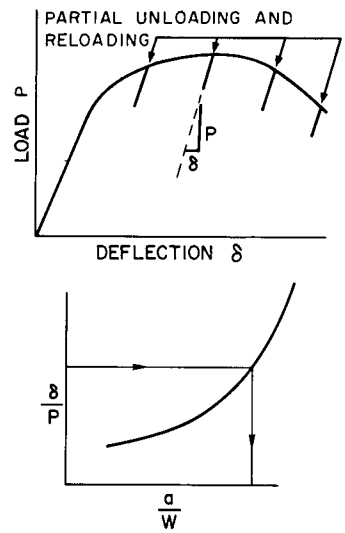

Fig. 11 — Procedure of determining a precise single-specimen compliance (δ/P) and then using a predetermined curve to predict the crack length (a/W)

The experimental procedure uses a CT specimen of E-399 proportions but having a modified notch geometry (Fig. 12) to permit the mounting of razor-sharp knife edges for measuring load line deflection with a clip gage. The notch modification has required a small increase in the distance between the hole centers of the E-399 standard specimen. The specimen is loaded with flat-bottom or D grips to minimize friction between the loading pin and the grip. Special techniques have been developed to permit remote loading of the specimen in a hot cell (Fig. 13). The specimen is heated by means of an electric-resistance oven; it is cooled below ambient temperature by circulating gaseous nitrogen. A thermocouple clamped to the specimen monitors the temperature during the test.

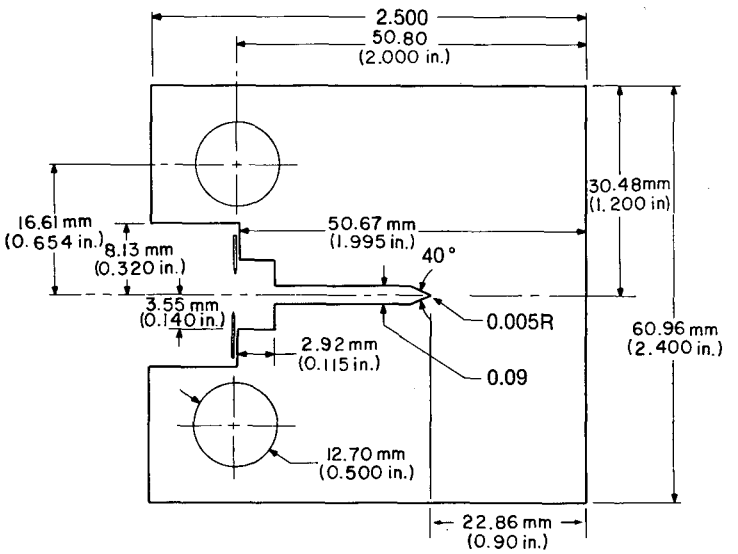

Fig. 12 — Geometry of a 1T compact specimen for an a/W of 0.6. In this program, however, a slightly shorter crack length (a/W = 0.5) has been used, as shown in Fig. 1. A precrack of 2.54 mm (0.100 in.) is added prior to testing.

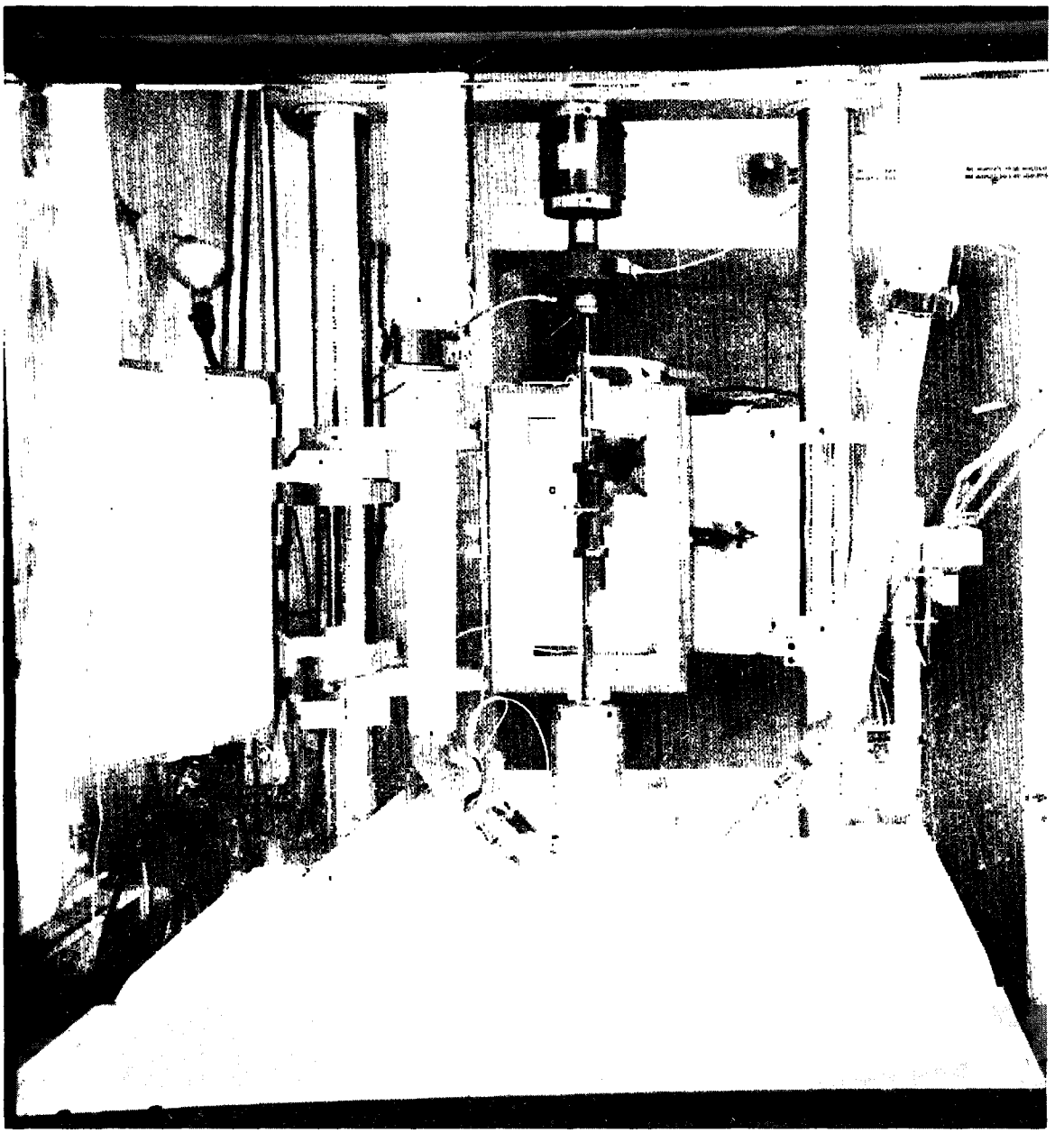

Fig. 13 — Experimental apparatus for J-integral testing by remote means in a hot cell

The specimen is loaded in an MTS servo-hydraulic machine. Load and load-line-deflection outputs are simultaneously fed into a computer and x-y plotters. The former permits an on-line determination of both J and the crack extension Δa. The computer code being used for the data reduction was originally developed by Joyce and Gudas [20] and subsequently modified by NRL.

A typical example of a load vs load-line displacement trace and of the magnified unload-load compliance traces taken from along this trace is provided in Figs. 14a and 14b respectively. From a repeatability viewpoint the specimen compliance records are accurate enough to detect crack length changes of ±0.08 mm (±3 mils) for a 1T specimen with an a/W of 0.5; the capability for crack length discrimination increases with longer cracks. However, repeatability is not to be confused with accuracy. The system accuracy is difficult to define, because it depends on the compounding of errors due to load-cell and clip-gage calibration factors, determination of Young's modulus, validity of the compliance expression used to translate the experimental compliance to specimen crack lengths, and the electronic noise level, which may vary between tests. (We take account of the clip-gage calibration factor, however, which exhibits a variation of approximately ±2.5% from the room-temperature value over the range of test temperatures used here. Failure to account for this will result in a corresponding error in the predicted Δa even when the results are normalized to force agreement with the optically measured precrack.) In spite of the compounding of errors, our development of the SSC method has resulted in a correspondence between predicted and measured *final* crack lengths, when these crack fronts are straight, to within 0.13 mm (5 mils). On the other hand, much larger discrepancies have been detected with smooth specimens having curved crack fronts and also with specimens exhibiting *straight* crack fronts which have been machined from an A302-B steel having a high nonmetallic inclusion content.

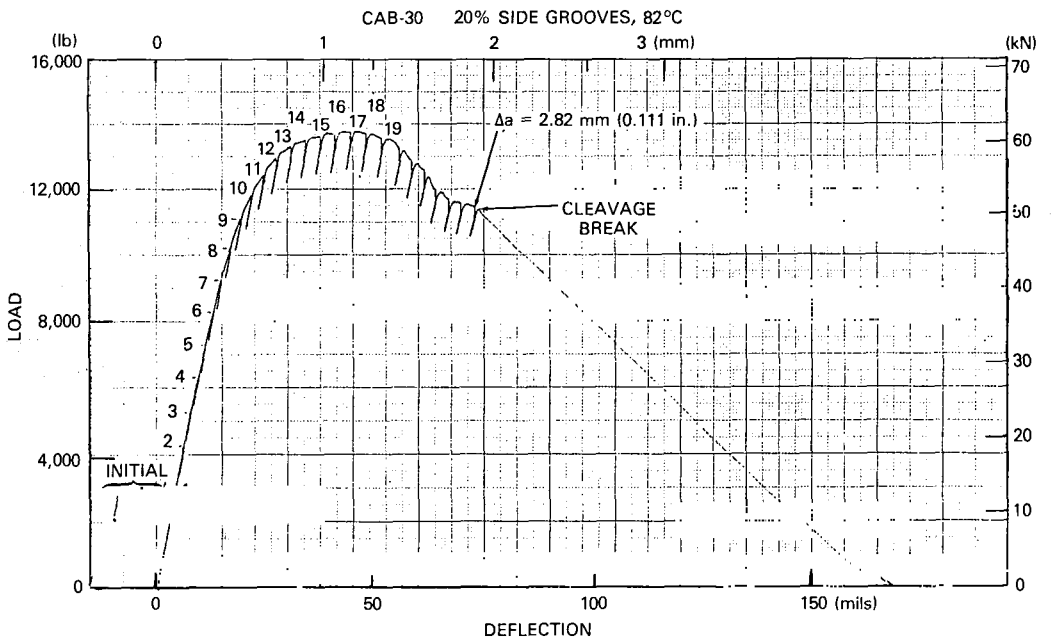

Fig. 14a — Load vs load-line-deflection record from the test of an irradiated specimen at 82°C (180°F) showing unstable fracture. Note the leveling of the curve prior to fracture.

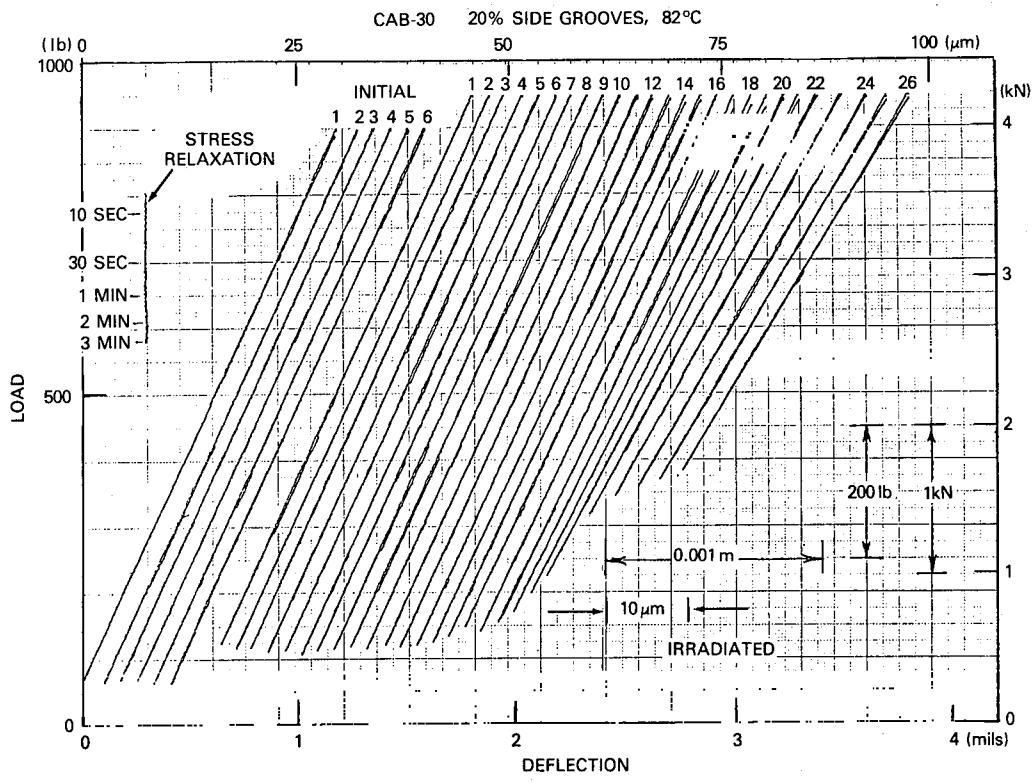

Fig. 14B — The unload-load traces taken from Fig. 14a and highly amplified. Hystereis is not noticeable. Also shown is an example of the load relaxation behavior while the specimen is held at constant deflection (upper left, for unloading 16).

The unloading traces (Fig. 14b) bear particular scrutiny, because they are the heart of the SSC method. As can be seen, there is no noticeable hysteresis. A least-squares fit of the unload-load slopes typically yields a 95% confidence limit of ±0.05 mm (2 mils).

Calculation of the J Integral

The value of J is computed from the expression

$$J = \frac{1 + \alpha}{1 + \alpha^2} \frac{2A}{B_N b_o}, \tag{3}$$

where A is the specimen energy input based on *total* deflection, b_o is the original unbroken ligament, B_N is the net thickness after the thickness B is reduced by the grooves, and the term $(1 + \alpha)/(1 + \alpha^2)$ is a modified Merkle-Corten correction to account for the tension component of the loading. (There is some disagreement as to whether the use of B_N is proper for side-grooved specimens. It has been suggested that a value between B and B_N may also be appropriate.) The modification of the Merkle-Corten correction from the original [21] has been derived by Clarke and Landes [22]. The simplicity of the modified correction is believed to override any minor loss in accuracy from the original expression. However, K_{Jc} values computed from Eq. (3) must also include the $1 - \nu^2$ term (Eq. (2)) to achieve the greatest accuracy [23], whereas this term should be omitted when the original Merkle-Corten correction is used.

Calculation of the Rotation Correction

As the loading progresses, minor rotations of the specimen result in corresponding reductions in the moment arm and in deviations of the clip-gage knife edge from the true load line (Fig. 15). A rotation correction has been derived to account for this behavior [24]:

$$(\delta/P)_c = \frac{(\delta/P)_m}{\left(\frac{H}{R}\sin\theta - \cos\theta\right)\left(\frac{D}{R}\sin\theta - \cos\theta\right)}, \tag{4}$$

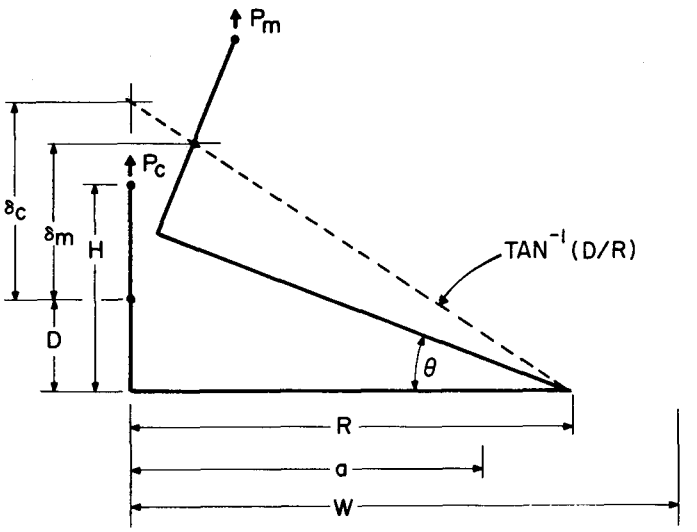

Fig. 15 — Elastic compliance correction for specimen rotation

where (Fig. 15)

δ = half-crack load-line displacement,
P = applied load,
c = value corrected for rotation,
m = value measured experimentally,
H = half span of the applied load points,
R = radius of rotation of the crack centerline at the measurement line when assuming a plastic hinge about the center of the uncracked ligament, $(W + a)/2$,
W = width of the specimen,
a = crack length from the load plane,
D = distance from the crack plane to the measurement line when $P = 0$,
θ = angle of rotation of a rigid body element about the unbroken midsection line, or

$$\theta = \sin^{-1}\left[(\delta_m + D)/(D^2 + R^2)^{0.5}\right] - \tan^{-1}(D/R).$$

Calculation of the Compliance

The value of crack length at selected points in the test is computed from the unload-load slope by means of a predetermined specimen compliance relationship. Two compliance relationships have been employed: the theoretical expression of Hudak et al. [25] based on a plane-stress assumption and an experimental compliance derived by NRL using blunt-notch specimens having different crack lengths [24]. A comparison of these two compliance trends (Fig. 16) shows the Hudak and experimental curves to be of a slightly different shape. For comparison, the Hudak and experimental curves in Fig. 16 have been forced to match at an a/W of 0.5. This was required, since the modulus of the specimens used for the experimental compliance was not precisely known. The difference

between the two compliances is not significant, and the two will predict nearly identical crack lengths when normalized to the same initial compliance for the fatigue precrack.

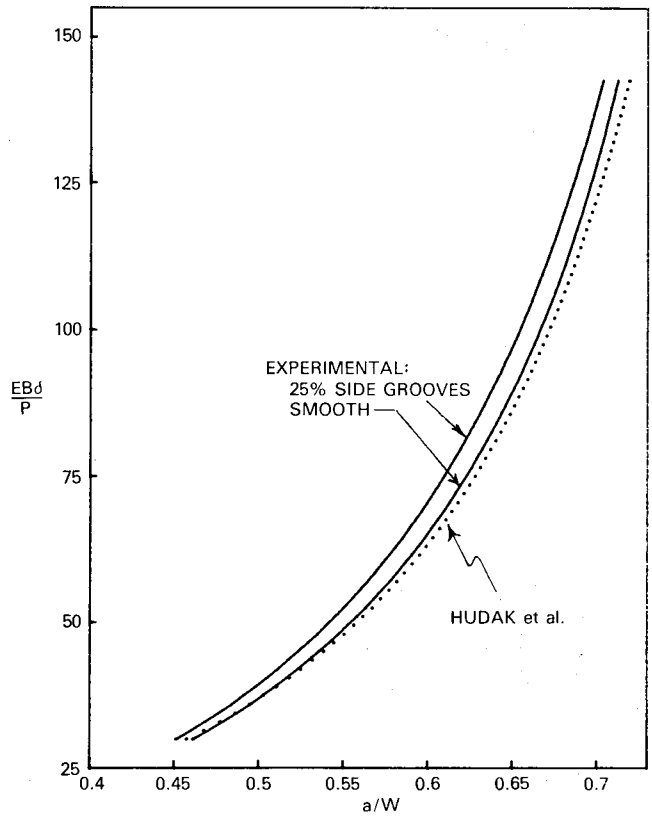

Fig. 16 — Comparison of the CT-specimen compliance relationship derived analytically by a plane-stress assumption (Hudak et al. [25] with that measured experimentally with blunt-notch specimens (smooth). The two curves have been matched at an a/W of 0.5. Also shown is the experimental compliance relationship for specimens having side grooves with 25% total depths.

The Hudak compliance applies only to smooth specimens. However, side grooves with depths of 10, 20, and 25% to eliminate the crack-front curvature were investigated. Hence an experimental blunt-notch compliance was also evolved by NRL for the specimens having 25% side grooves. A comparison between the experimental compliance of smooth and side grooved specimens (Fig. 16 shows that both curves are similar in shape but displaced slightly along the vertical axis. On the basis of this behavior we would infer a similar result for a theoretical compliance for side-grooved specimens. In practice, the 25%-side-groove compliance is used for the specimens having 20 to 25% side grooves, and the smooth-specimen compliance is used for the specimens having 0 and 10% side grooves.

To compute the absolute crack length from the compliance, it is necessary to know the modulus as well as the δ/P slope. The modulus is a function of test temperature and is generally not known exactly. To avoid this problem, agreement is forced between the length of the specimen fatigue precrack as predicted by the SSC method and as measured optically; this agreement defines a match modulus which is then used for subsequent crack length predictions. This procedure is not to be construed as a method for determining modulus but only as a means to an end. With this initialization of the precrack length, the previously stated accuracy in the predicted final crack is obtained.

Effect of Side Grooves

The side grooves were machined with a Charpy V-notch cutter having a 45° included angle and a 0.25-mm (0.010-in.) root radius. Figure 17a compares the crack-front shape for 0 and 10% side grooves in specimens from an A533-B steel plate (code CBB). It is clear that 10% side grooves have had little effect in straightening the crack front. However, one can observe a slight tendency for a reverse crack-front curvature where the crack front intersects the side grooves.

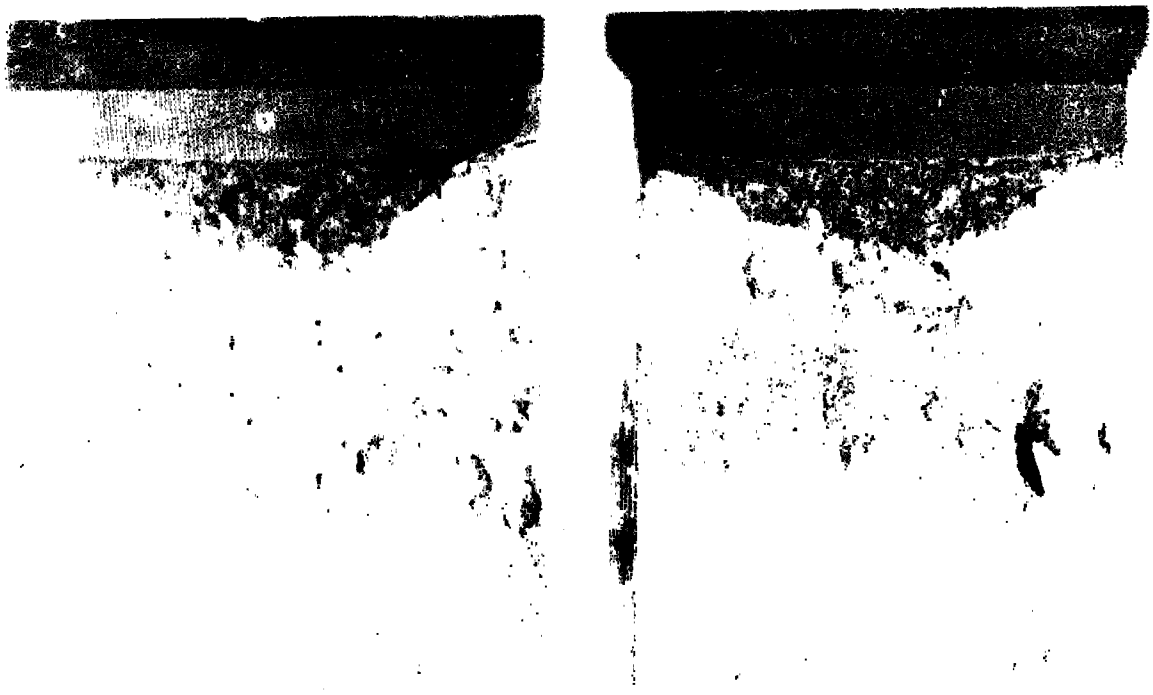

Fig. 17a — Comparison of crack-front curvature resulting from 0 and 10% side grooves in A533-B steel 1T-CT specimens cut from the plate of foreign production. The curvature of the heat-tinted crack tends to reverse near the grooves in the side-grooved specimen

Figure 17b compares crack-front curvature between specimens cut from another A533-B plate (code CAB) and having 20 and 25% side grooves. The crack fronts illustrated here exhibit much less curvature than that associated with the 10% side grooves. There appears to be little difference in crack-front curvature between specimens having 20 or 25% side grooves. This conclusion is also reflected in the similarity of the R-curve shape from these specimens, as discussed later.

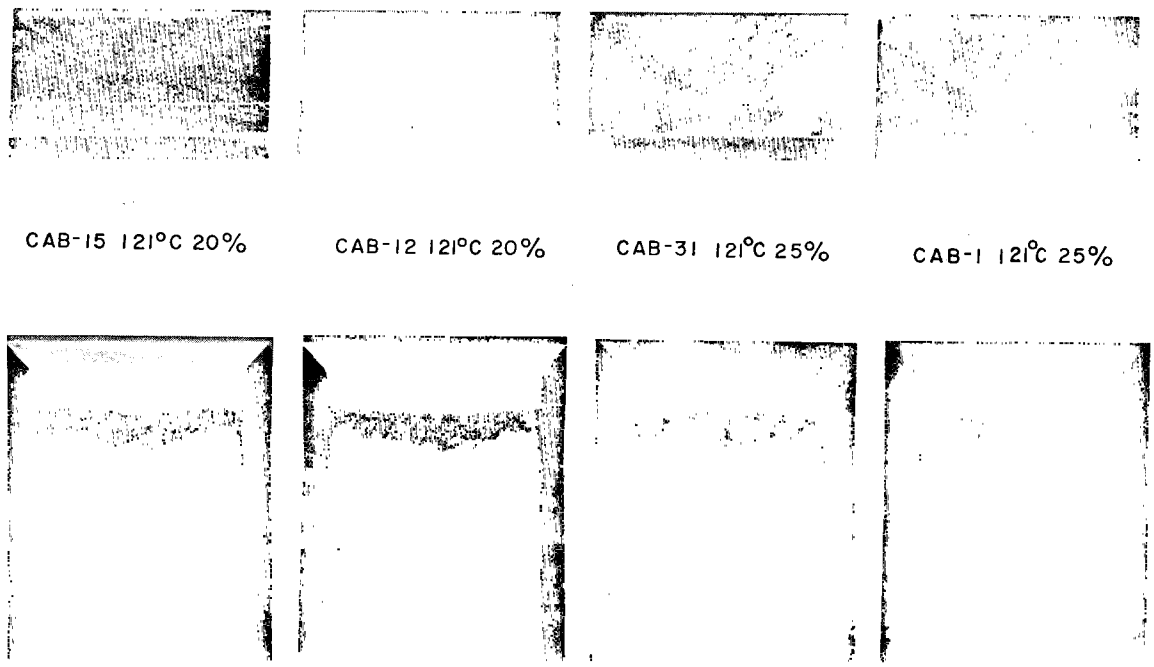

Fig. 17b — Comparison of crack-front curvatures resulting from 20 and 25% side grooves in 1T-CT specimens cut from A533-B steel plate of U.S. production. Straight crack fronts appear to result from the 25% side grooves, but the improvement over the crack fronts resulting from the 20% side grooves is minimal

Finally Fig. 17c contrasts the crack-front curvature which results from 20% side grooves in specimens cut from an A533-B plate and an A533 submerged arc weld (NRL code V86); the latter specimen was tested in conjunction with an NRC-sponsored program. There is a tendency for reverse tunneling in the weld metal specimen but a barely noticeable tendency in the plate specimen. Thus it appears that the degree of side grooving required to straighten the crack front is not a constant but depends on the material. For this program we have determined that 20% side grooves will produce the desired result.

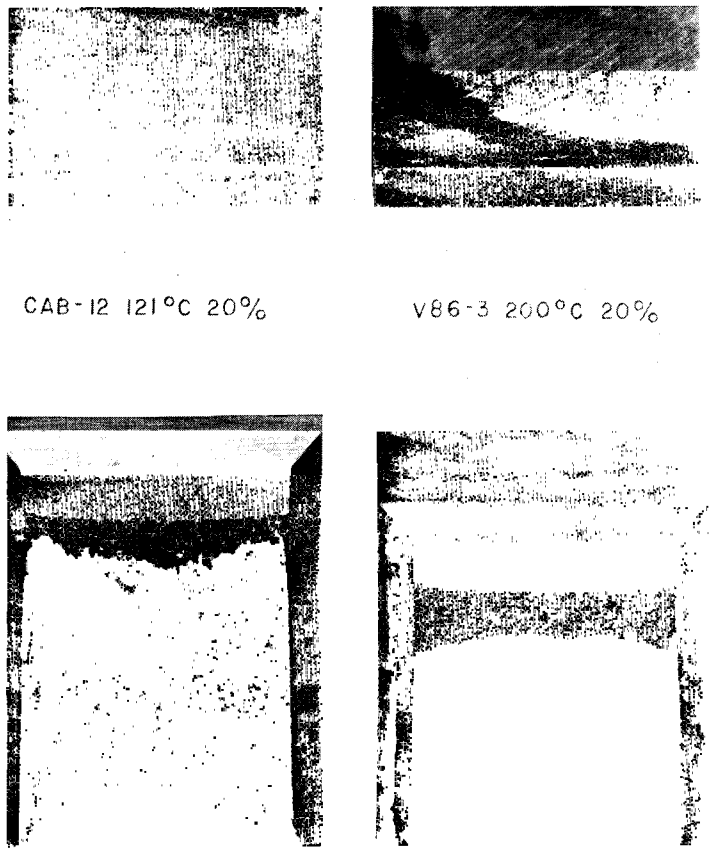

Fig. 17c — Effect of 20% side grooves in 1T-CT specimens cut from plate (left) and weld metal (right). The influence of side grooves in straightening the crack front appears to be alloy dependent. Reverse tunneling of the crack front occurs in the weld metal. However, this reversal in the plate results in a barely noticeable gull shape.

Alternative J_{Ic} Measurement

Figure 18 illustrates a typical *J-R* curve for plate CAB at the temperature of the upper shelf. The J_{Ic} value is currently defined by the proposed ASTM standard method [16] as the intersection of the blunting line with the least-squares fit of the points lying between the parallel dashed lines. The left dashed line is termed an exclusion line. This is believed to be an indicator of the first real crack extension. In other words, any crack extension less than the exclusion line is difficult to distinguish from blunting.

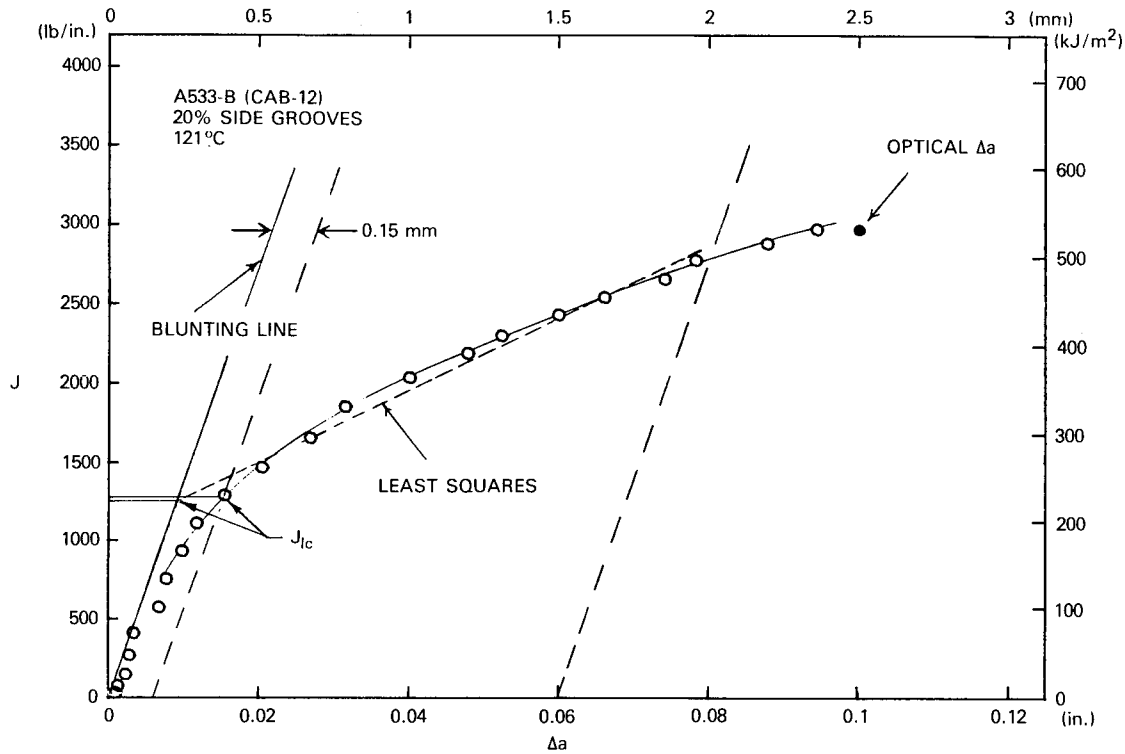

Fig. 18 — Typical R curve exhibiting a curved behavior. An alternative definition of J_{Ic} is the intersection of a smoothly drawn R curve and an exclusion line drawn 0.15 mm to the right of the blunting line. Also shown is the proposed ASTM definition of J_{Ic} as illustrated in Fig. 10

In the present program many of the tests will exhibit only a limited degree of stable (ductile) crack extension, followed by brittle failure (cleavage instability), such as indicated in Fig. 19. For these cases the R curve will be too limited to determine J_{Ic} via a least-squares fit of the data. (If Δa at failure is less than twice the extension to the blunting line, J_{Ic} by the ASTM procedure is taken as the value at instability.) On the other hand these specimens exhibit sufficient plasticity so as to be grossly invalid by a K_{Ic} criterion (E-399). Consequently data of this type cannot be interpreted easily by current or proposed standards.

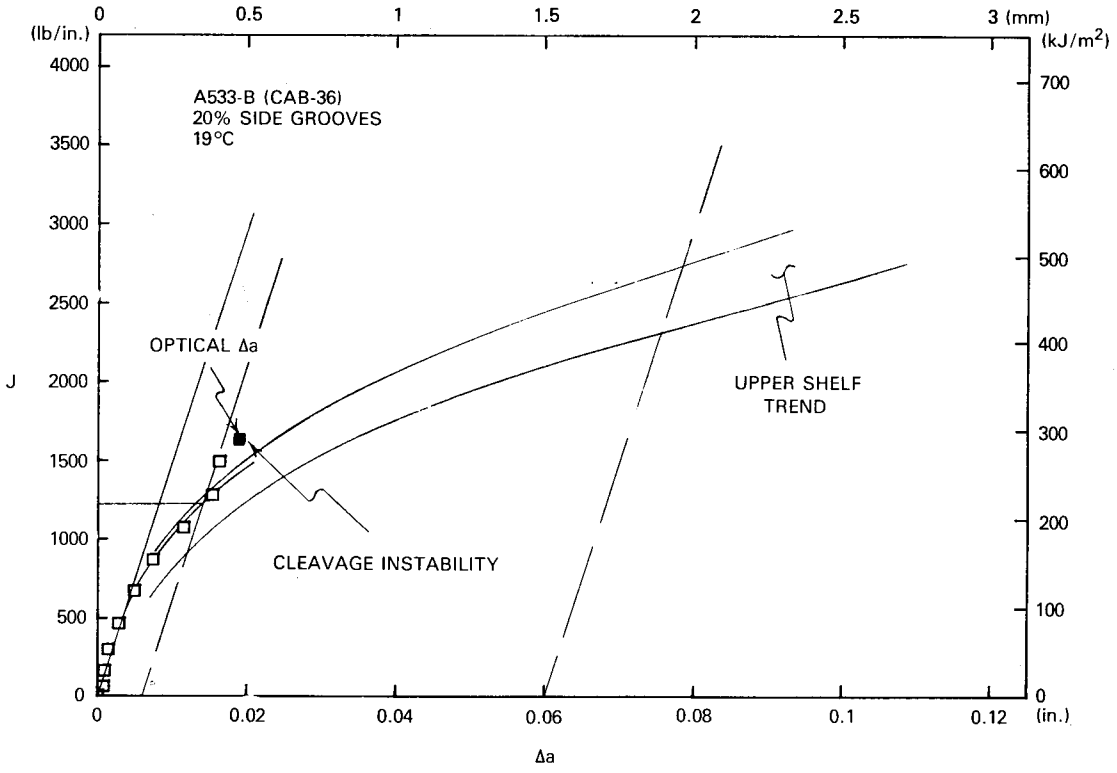

Fig. 19 — The R curve for a specimen which exhibited a limited stable crack extension prior to brittle fracture. The shape of the R curve sharply increases prior to fracture. (The upper shelf trend is from Fig. 20 and will be discussed in connection with that figure.)

If Δa at failure is greater than twice the extension to the blunting line, the ASTM definition of J_{Ic} can be applied. However, the R curve in Fig. 18 exhibits a nonlinear behavior, especially in the region near the blunting line. Because of this curvature, a least-squares fit of only a few of the points to the right of the exclusion line in Fig. 18 would result in a steeper line than the least squares fit of all the points. The result could be a J_{Ic} value at least 20% below that shown in Fig. 18. There appears to be no physical basis to justify such differences in J_{Ic}, thereby suggesting a deficiency in the ASTM definition.

Because of the behavior illustrated in the preceding examples, an alternative measurement procedure for J_{Ic} has been formulated as also shown in Fig. 18. This procedure involves substituting a smooth curve through the data in place of a linear regression, with J_{Ic} then being defined by the intersection of this curve with the 0.15-mm exclusion line. The choice of the exclusion line as part of the J_{Ic} definition criterion is based on the association of this line with the first indication of crack extension from a practical viewpoint as implied by Ref. 16. The advantage of the alternative method is that it will define the same J_{Ic} value irrespective of the amount of crack extension prior to fracture or the degree of R-curve curvature, thereby circumventing the difficulties encountered with the proposed ASTM procedure. In addition, for a large crack extension the alternative definition

of J_{Ic} may also yield values comparable with those defined by the ASTM procedure. In Fig. 18 for example both methods define essentially the same J_{Ic}.

In the case of specimen failure at crack extensions less than those defined by the exclusion line, J_{Ic} is computed at the level of failure. This approach is consistent with that normally taken for this type of behavior. For example, tests with plate CAB for which the J at failure was equated with J_{Ic} have produced measurable extensions, including blunting, of 0.05 to 0.25 mm (2 to 10 mils). For the J_{Ic} level indicated in Fig. 18, this amount of crack extension is less than that defined by the exclusion line and is therefore considered negligible.

R-Curve Trends

Figure 20 compares R curves from plate CAB in the C_v upper shelf regime using one specimen having 20% side grooves and two specimens having 25% side grooves. The curves exhibit relatively little scatter; this behavior is consistent with the relatively straight crack fronts for the 20 and 25% side-grooved specimens illustrated in Fig. 17b. The range of J_{Ic} values for these specimens using the alternative definition is 182 to 223 kJ/m^2 (1040 to 1275 lb/in.). This compares with a J_{Ic} range of 171 to 221 kJ/m^2 (974 to 1263 lb/in.) by the proposed ASTM definition. When Eq. (2) and the alternative definition of J_{Ic} are used, a mean value for K_{Jc} of 211 MPa$\sqrt{\text{m}}$ (192 ksi$\sqrt{\text{in.}}$) is obtained on the upper shelf.

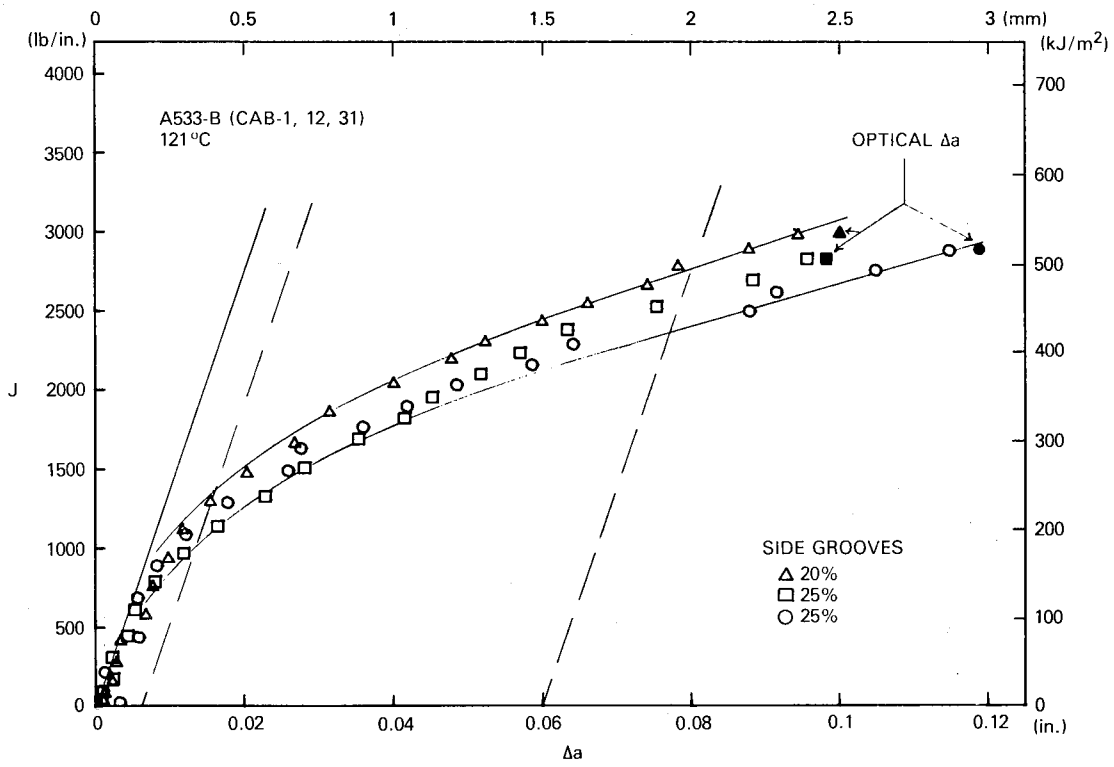

Fig. 20 — Comparison of R curves in the upper shelf temperature region for three specimens. The predicted final crack lengths agree with the measured (optical) crack lengths

For specimens having stable growth prior to a cleavage instability, the R curve shows an unexpected behavior which has not been previously observed. As illustrated in Fig. 19, the R curve exhibits a sharp increase in slope just prior to fracture. In cases such as this, the definition of J_{Ic} by a least-squares fit of the data would be clearly inappropriate. This test is typical of other results with plate CAB and appears to reflect a hardening prior to cleavage failure. This has been associated with a leveling of the load-versus-deflection record after the maximum load, as shown in Fig. 14a. (Since the specimen in Fig. 19 failed at the maximum load, this hardening was not distinguished on the load-versus-deflection record).

For the specimen in Fig. 19 the J_{Ic} value is defined by the intersection of the smoothly drawn R curve with the exclusion line. In other words, the final SSC data point has been ignored. With this specimen a direct comparison is not possible between the last SSC point and the point based upon the optically measured Δa. This R curve, with the exception of the anomalous behavior at fracture, fits within the trend of R curves at the upper shelf shown in Fig. 20.

The crack extension values presented here are based on an experimental compliance relationship (Fig. 16). Figure 21a compares the J-R curves which result from an application of the Hudak et al. and experimental compliance expressions. The differences resulting from the application of the two compliance relationships is slight and for this example amounts to an 8% change in J_{Ic} and in the R-curve slope.

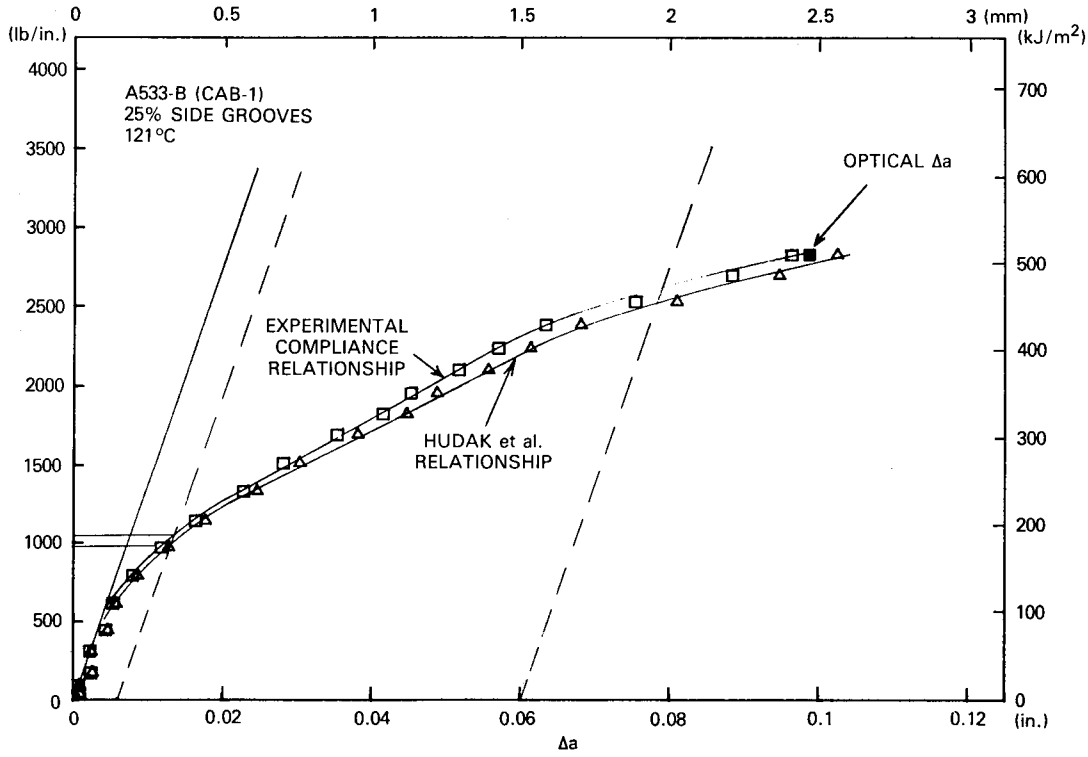

Fig. 21a — Comparison of R curves (with the specimen rotation correction of Eq. (4)) computed on the basis of the theoretical and experimental (25% side grooves) compliance relationships shown in Fig. 16

Figure 21b illustrates the result of applying the correction for specimen rotation (Eq. (4)). The J_{Ic} value is reduced by 15% as a result of this correction. However, there is little difference in the tearing modulus. As expected, the final measured crack length agrees better with the predicted values after the rotation correction has been applied.

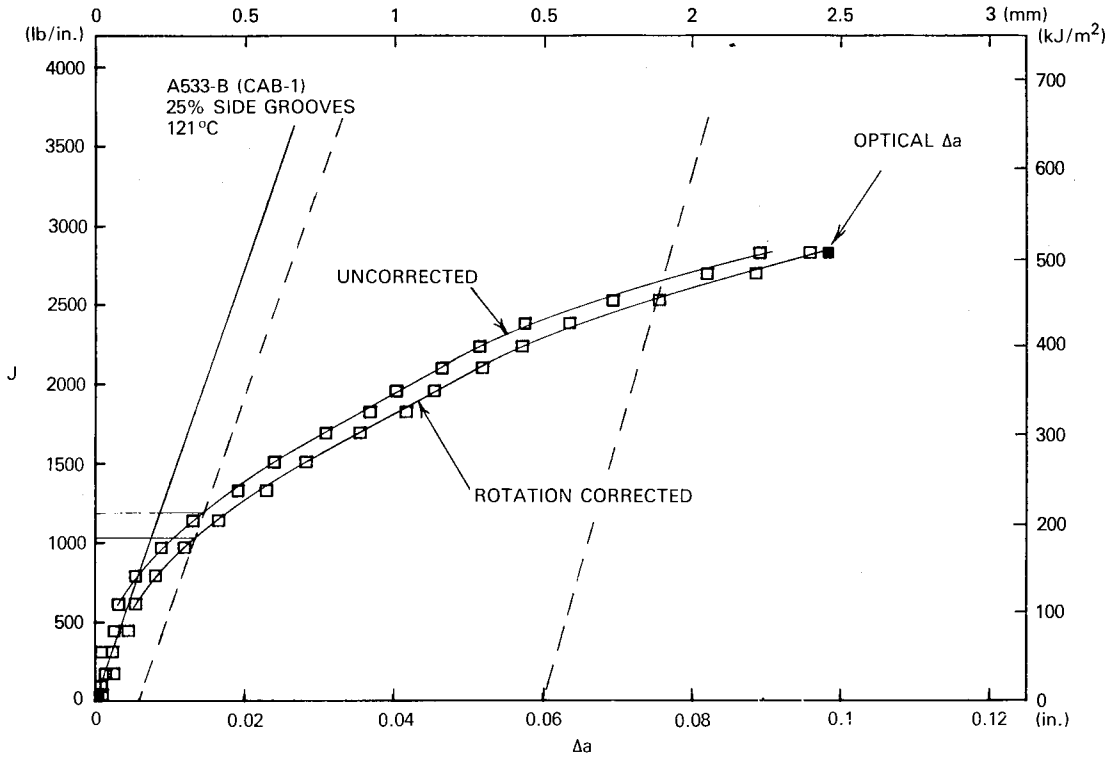

Fig. 21b — Effect of the specimen rotation correction of Eq. (4) for a typical R curve (computed on the basis of the experimental compliance relationship shown in Fig. 16)

Upper Shelf Definition

A comparison of Figs. 19 and 20 suggests that the R-curve shape is influenced very little by temperature over a 100°C (180°F) interval. Consequently, once the R curve crosses the exclusion line, essentially the same value of J_{Ic} will be defined, within experimental scatter, regardless of whether the specimen exhibits fibrous tearing or cleavage instability as a consequence of further crack extension beyond this level. It is proposed, therefore, that an "upper shelf initiation toughness" be defined as that level where a crack extension of 0.15 mm is first achieved.

Some confusion may result when this definition is contrasted with that normally associated with C_v upper shelf behavior. The latter refers to the temperature region of completely fibrous fracture of the C_v specimen. The J_{Ic} upper shelf definition is consistent with this concept in that the crack extension between the blunting and exclusion lines will also be primarily fibrous. (The possibility of some cleavage on a microscale is possible, but from a practical viewpoint this behavior, if it occurred, has had no effect on the R-curve example in Fig. 19). With this definition of an upper shelf J_{Ic}, however, one must allow for the possibility of cleavage instability *after* the initiation toughness has been achieved; the latter phenomenon is important to structural integrity and must be considered separately in terms of a stability analysis.

Postirradiation CT Specimen Evaluations
F.J. Loss, B.H. Menke, and R.A. Gray, Jr.

R Curve of Irradiated Material

In CY-1978, tests have been conducted with selected specimens from experiments BSR-2 and BSR-3. Side grooves of 20% depth were machined in all specimens after irradiation. Most of these specimens failed without measurable crack extension; therefore *J-R* curves were not produced. However, an example for one of the tests which did show significant crack extension prior to brittle fracture is presented in Fig. 22. The *R* curve for this specimen exhibits a change in slope prior to fracture similar to that illustrated in Fig. 19.

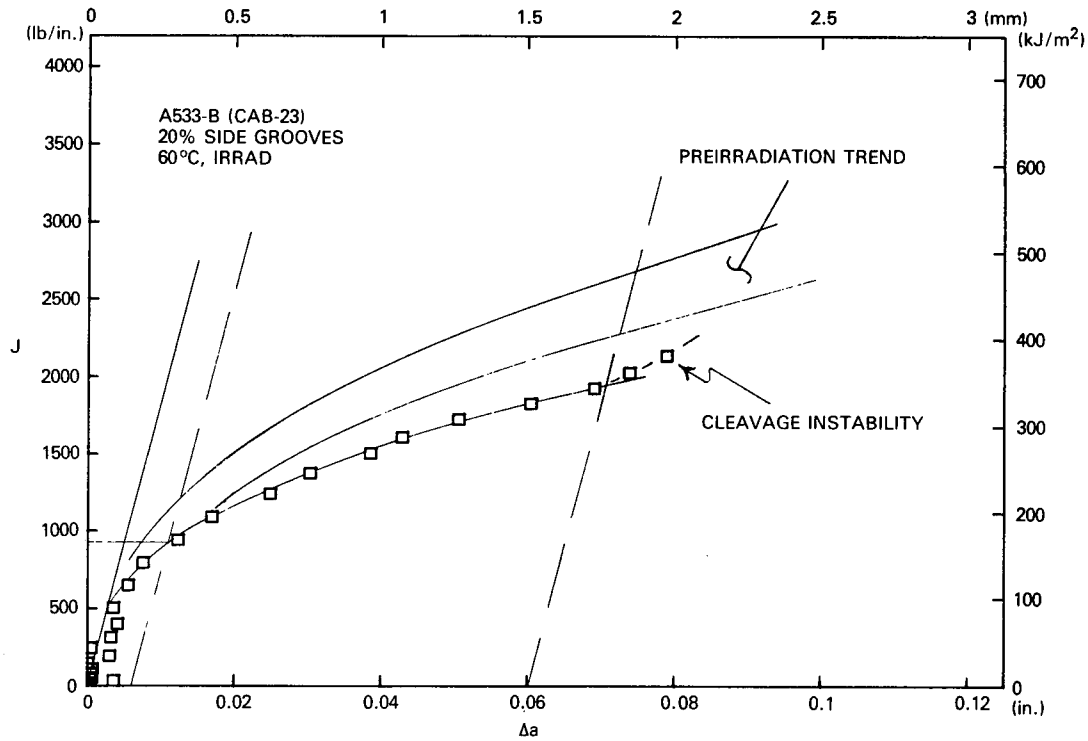

Fig. 22 — The *J-R* curve behavior of irradiated material from the BSR-2 capsule. The trend of unirradiated material (Fig. 20) is shown for comparison

By the previous analysis the specimen in Fig. 22 is considered to represent upper shelf behavior for the irradiated steel even though a cleavage fracture was observed. The initial position of the *R* curve is within the scatterband for unirradiated tests in the upper shelf regime. Thus the upper shelf toughness for the code CAB material from the BSR—2 irradiation is changed very little from the unirradiated condition. Actually, however, a small (10%)

decrease in K_{Jc} for the irradiated material is determined, because the higher flow stress of the irradiated material causes a steeper exclusion line to be drawn; this results in an intersection with the R curve at a lower value of J. On the other hand the tearing modulus shows a larger degradation with irradiation (a factor of 2.3) than is experienced with J_{Ic}. This behavior is observed qualitatively by comparing the R-curve slopes in Fig. 22.

Comparison of Preirradiation and Postirradiation Fracture Toughness

Figure 23 presents a comparison of the initiation toughness K_{Jc} for the irradiation and unirradiated conditions of plate CAB. All of the specimens except for the three tested at 121°C (250°F), failed in a cleavage mode after some amount of ductile crack extension. This figure also presents a comparison with the unirradiated tests conducted by Combustion Engineering (CE) in an earlier EPRI-sponsored program [26]. Agreement is good between the results of the two laboratories.

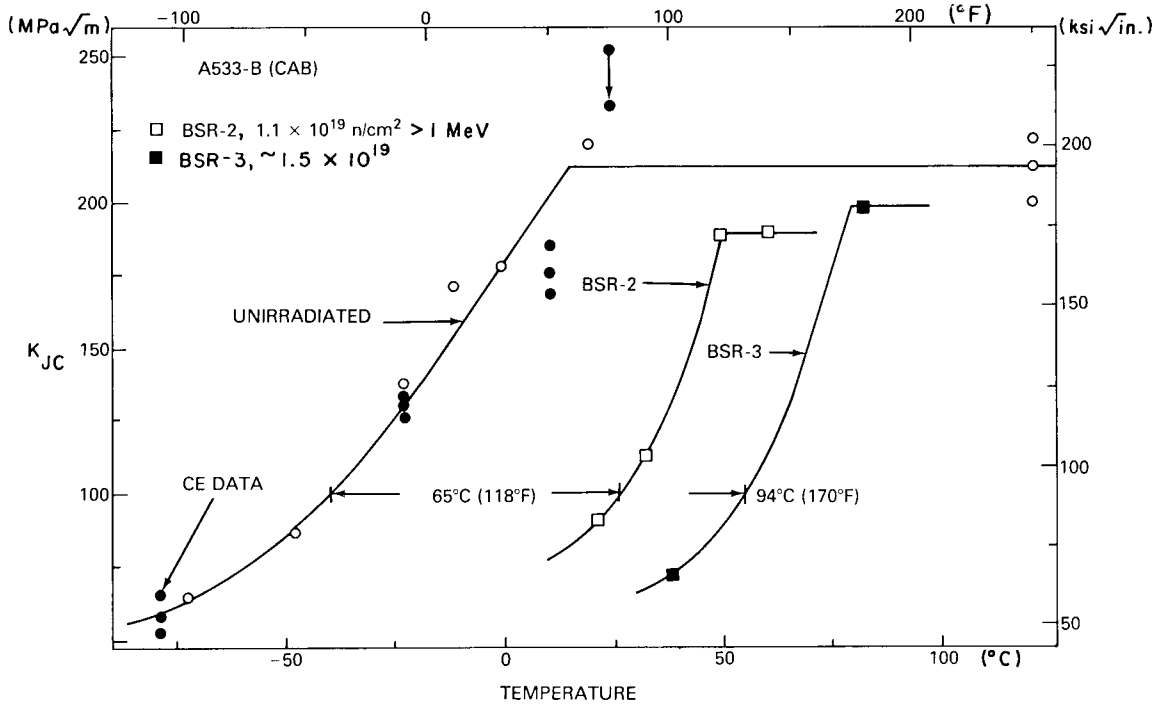

Fig. 23 — Comparison of preirradiation and postirradiation fracture toughness from J-integral analysis for an A533-B steel. The unirradiated toughness measured by Combustion Engineering, Inc. [26], is also plotted (filled circles).

The highest CE data point, at 24°C (75°F), was the test of a 2T-CT specimen, and its toughness was computed from the J integral to the maximum load in accordance with Eq. (2). NRL has measured the average crack extension (including blunting) from the specimen surface as 0.6 mm (22 mils). Coincidentally this value of Δa, coupled with the J value at fracture determined by CE, falls close to the highest R curve in Fig. 20. The resulting J_{Ic} by the alternative definition produces a K_{Jc} which is similar to the values measured by NRL at both 19°C (66°F) and 121°C (250°F). Therefore we have adjusted downward this CE data point as shown in Fig. 23.

In Fig. 23 the curve for the unirradiated condition sharply changes slope between the transition and upper shelf regions as opposed to the smooth curve between these regions normally exhibited by conventional C_v trends. This slope change follows from the alternative definition of J_{Ic}. At crack extensions less than those defined by the exclusion line, fracture proceeds in a cleavage mode with little or no real crack extension. When this occurs, K_{Ic} is determined from the J value at fracture; this process results in the trend of increasing K_{Jc} with temperature. As the crack extension exceeds the exclusion line, K_{Jc} remains essentially constant. This type of K_{Ic}-versus-temperature curve is believed to be a general curve applicable to other steels which exhibit a micromode fracture transition from cleavage to fibrous. Not unexpectedly the PCC_v curves previously presented also exhibit this general shape.

A measure of the toughness degradation with irradiation is often denoted by a temperature shift (ΔT) at some arbitrary toughness level in the transition region, such as 100 MPa$\sqrt{\text{m}}$ (91 ksi$\sqrt{\text{in.}}$). In Fig. 23 the temperature shift at this toughness is 65°C (118°F) for the BSR-2 irradiation capsule and 94°C (170°F) for the BSR-3 irradiation capsule. These ΔT values are in good agreement with those defined by the PCC_v test at a similar toughness level. The C_v temperature shifts at the 41-J (30 ft-lb) level are somewhat less than these values. Small fluence differences within the specimen irradiation assembly may have contributed to differences in PCC_v-versus-C_v or CT-versus-C_v measurements of the irradiation effect.

Summary of CT Specimen Evaluations

The single-specimen compliance technique has been applied to define the J-R curve and J_{Ic} trends of an A533-B plate (code CAB) in both preirradiation and postirradiation conditions. An important conclusion was that J_{Ic} appears to lack sufficient precision to resolve J_{Ic} values for material exhibiting a brittle instability (cleavage) preceded by a small amount of ductile crack extension. An alternative experimental definition for J_{Ic} was formulated to resolve this problem. In addition it was concluded that a small (8%) difference in J_{Ic} and R-curve slope exists between the analyses based on theoretical and experimental specimen compliance and that a rotation correction for J can result in a reduction of 15% in J_{Ic}.

On the basis of physical behavior it is suggested that the trend of K_{Jc} versus temperature should sharply change slope to denote the border between the upper shelf and transition regions. Brittle fracture is shown to occur on the upper shelf albeit preceded by a limited amount of stable crack extension. This phenomenon suggests caution in the structural interpretation of upper shelf behavior. The irradiated upper shelf toughness

K_{Ic} for code CAB material from the BSR-2 capsule exhibited only a 10% degradation in comparison with the unirradiated level. On the other hand the tearing modulus was reduced by a factor of 2.3 with irradiation. This suggests that the interpretation of upper shelf toughness should not be based solely on an initiation toughness.

With the BSR-2 and BSR-3 irradiated specimens a temperature elevation of 65 and 94°C respectively was observed in the transition temperature regime at a toughness level of 100 MPa$\sqrt{m}$. These values are in general agreement with those projected from PCC_v trends at the same toughness level.

Thermal Control Tests

J.R. Hawthorne

Long-term 288°C heating effects in the absence of nuclear radiation will be determined with thermal control specimens. Thermal conditioning treatments for all materials were scheduled to commence in CY 1979. All four specimen types (C_v, PCC_v, CT, and tensile) will be included in limited numbers. Initially only one thermal conditioning time will be evaluated for each material and will correspond to the longest expected time at temperature in the reactor (highest fluence condition). Additional, shorter thermal conditioning times will be considered if first results warrant. Exposure times for experiments BSR-2, BSR-3, BSR-4, and BSR-5 were respectively 22.4, 34.6, 76.2, and 71.9 days. The longest time of exposure for planned experiments is not expected to exceed 92 days (2200 hours). Initial results from thermal control tests will become available in September 1979. Thermal control investigations should be completed by February 1980.

PLANS FOR CY 1979

Experimental plans for CY 1979 include the following efforts and objectives:

- Completion of reactor irradiation exposures for experiments BSR-6 through BSR-14. (The material for experiment BSR-14 will be decided in part from the results of experiments BSR-2 through BSR-10).

- Completion of computer calculations of neutron spectrum conditions in the NRL-EPRI experiment irradiation facilities (BSR core positions 76 and 78).

- Completion of preirradation and postirradiation C_v, PCC_v, and tensile tests (all materials).

- Completion of thermal conditioning treatments and commencement of postconditioning tests (all materials).

- Continuation of preirradiation and postirradiation CT specimen testing (all materials).

- Evaluation of C_v and PCC_v test methods correlation for the irradiated condition.
- Development of the initial correlation test of C_v-versus-CT test methods.

Research findings and accomplishments during this period will be documented in the third annual progress report.

ACKNOWLEDGMENTS

The authors express their appreciation to Dr. T. U. Marston of EPRI for his guidance of the research program and his assistance in securing program materials. The authors also thank L. E. Steele of NRL for his support on program administration. The important contributions of J. D. Forsyth, W. E. Hagel, and T. A. Zimmerman to certain phases of the experimental program are acknowledged also with gratitude.

REFERENCES

1. J.R. Hawthorne, editor, "The NRL-EPRI Research Program (RP886-2), Evaluation and Prediction of Neutron Embrittlement in Reactor Pressure Vessel Materials, Annual Progress Report for CY 1977," NRL Memorandum Report 3734, Mar. 1978.
2. J.R. Hawthorne, "Radiation Effects Information Generated on the ASTM Reference Correlation-Monitor Steels," ASTM DS-54, American Society for Testing and Materials, July 1974.
3. T.U. Marston, M.P. Borden, J.H. Fox, and L.D. Reardon, "Fracture Toughness of Ferritic Materials in Light Water Nuclear Reactor Vessels," Combustion Engineering, Inc., Power Systems Division, EPRI 232-2, Oct. 1975.
4. W.A. Van Der Sluys, R.R. Seeley, and J.E. Schwabe, "Determining Fracture Properties of Reactor Vessel Forging Materials, Weldments and Bolting Materials," The Babcock and Wilcox Company, EPRI NP 122, July 1976.
5. W.L. Server and W. Oldfield, "Nuclear Pressure Vessel Steel Data Base," Fracture Control Corporation, EPRI NR 933, Dec. 1978.
6. Quality Engineering Branch, Army Materials and Mechanics Research Center, personal communication, 30 Nov. 1977.
7. Quality Engineering Branch, Army Materials and Mechanics Research Center, personal communication, 23 Oct. 1978.
8. Quality Engineering Branch, Army Materials and Mechanics Research Center, personal contribution, 20 Oct. 1978.
9. Quality Engineering Branch, Army Materials and Research Center, personal communication, 6 July 1978.

10. J.R. Hawthorne, J.J. Koziol, and R.C. Groeschel, "Evaluation of Commercial Production A533-B Plates and Weld Deposits Tailored for Improved Radiation Embrittlement Resistance," pp 83-102 in *Properties of Reactor Structural Alloys After Neutron or Particle Irradiation*, ASTM STP 570, Feb. 1976.

11. "Effects of Residual Elements on Predicted Radiation Damage to Reactor Vessel Materials," Regulatory Guide 1.99, U.S. Nuclear Regulatory Commission, Office of Standards Development, Washington, D.C., Apr. 1977.

12. J.R. Hawthorne, "Demonstration of Improved Radiation Embrittlement Resistance of A533-B Steel Through Control of Selected Residual Elements," NRL Report 7121, May 1970.

13. J.R. Hawthorne, "Contributions of Selected Residual Elements to the Radiation Embrittlement Sensitivity of Steel Forgings," NRL Report 7526, Jan. 1973.

14. D.R. Ireland, W.L. Server, and R.A. Wullaert, "Procedures for Testing and Data Analysis, Task A — Topical Report," Effects Technology, Inc., ETI Technical Report 75-43, Oct. 1975, pp 5-1 through 5-52.

15. D.R. Ireland, W.L. Server, and R.A. Wullaert, "Procedures for Testing and Data Analysis, Task A — Topical Report," ETI Technical Report 75-43, Oct. 1975, p 5-46.

16. "The Determination of the Elastic-Plastic Toughess Parameter, J_{Ic}," ASTM Committee E24.08.04, 12 Mar. 1979.

17. P. Paris, H. Tada, A. Zahoor, and H. Ernst, "A Treatment of the Subject of Tearing Instability," NUREG-0311, Nuclear Regulatory Commission, Aug. 1977.

18. G.A. Clarke, W.R. Andrews, P.C. Paris, and D.W. Schmidt, "Single Specimen Tests for J_{Ic} Determination," American Society for Testing and Materials, ASTM STP 590, 1976, pp 27-42.

19. G.R. Irwin, "Comments on J_{Ic} and *J-R* Testing," 16 Mar. 1979, unpublished.

20. J.A. Joyce and J.P. Gudas, "Computer Interactive J_{Ic} Testing of Navy Alloys," American Society for Testing and Materials, ASTM STP 668, Apr. 1979, pp 451-468.

21. J.G. Merkle and H.T. Corten, "A *J* Integral Analysis for the Compact Specimen, Considering Axial Force as Well as Bending Effects," Journal of Pressure Vessel Technology, Trans. ASME J96, 286-292 (Nov. 1974).

22. G.A. Clarke and J.D. Landes, "Evaluation of *J* for the Compact Specimen," Scientific Paper 78-1D3-JINTF-P1, Westinghouse R&D Center, 12 June 1978.

23. F.J. Loss, unpublished data.

24. F.J. Loss, editor, "Structural Integrity of Water Reactor Pressure Boundary Components — Progress Report Ending 30 Nov 1977," NRL Memorandum Report 3782, May 1978.

25. S.J. Hudak, Jr., A. Saxena, R.J. Bucci, and R.C. Malcolm, "Development of Standard Methods of Testing and Analyzing Fatigue Crack Growth Rate Data — Final Report," Air Force Material Laboratory, AFML TR 78-40, 10 Mar. 1977.

26. T.U. Marston, M.P. Borden, J.H. Fox, and L.D. Reardon, "Fracture Toughness of Ferritic Materials in Light Water Nuclear Reactor Vessels — Final Report," EPRI Contract RP232-2, Combustion Engineering, Inc., 13 Oct. 1975.